



# Discontinuous crack-bridging model for fracture toughness analysis of nacre

Yue Shao<sup>a,1</sup>, Hong-Ping Zhao<sup>a</sup>, Xi-Qiao Feng<sup>a,\*</sup>, Huajian Gao<sup>b</sup>

<sup>a</sup> Center for Nano and Micro Mechanics & Institute of Biomechanics and Medical Engineering, Department of Engineering Mechanics, Tsinghua University, Beijing 100084, China

<sup>b</sup> School of Engineering, Brown University, Providence, RI 02912, USA

## ARTICLE INFO

### Article history:

Received 23 June 2011

Received in revised form

17 April 2012

Accepted 20 April 2012

Available online 27 April 2012

### Keywords:

Biological material

Microstructure

Crack

Size effect

Biomimetics

## ABSTRACT

Studying the structure–property relation of biological materials can not only provide insight into the physical mechanisms underlying their superior properties and functions but also benefit the design and fabrication of advanced biomimetic materials. In this paper, we present a microstructure-based fracture mechanics model to investigate the toughening effect due to the crack-bridging mechanism of platelets. Our theoretical analysis demonstrates the crucial contribution of this mechanism to the high toughness of nacre. It is found that the fracture toughness of nacre exhibits distinct dependence on the sizes of platelets, and the optimized ranges for the thickness and length of platelets required to achieve higher fracture toughness are given. In addition, the effects of such factors as the mechanical properties of the organic phase (or interfaces), the effective elastic modulus of nacre, and the stacking pattern of platelets are also examined. Finally, some guidelines for the biomimetic design of novel materials are proposed based on our theoretical analysis.

© 2012 Elsevier Ltd. All rights reserved.

## 1. Introduction

As a result of evolution over many millions of years, most biological materials in plants and animals have combined multiple physical merits to fulfill their biological functions. The physical and mechanical properties of a biological material are determined not only by its chemical compositions but also by its structures at multiple length scales, which have been selected according to the basic rules of evolution and optimization in nature. Investigation of these natural materials can provide biological inspirations to revolutionize the techniques for producing novel materials with improved properties and functions. In recent years, therefore, considerable experimental and theoretical efforts have been directed toward understanding the composition–structure–property–function relations of some representative biological materials, e.g., bones, teeth, horns, mollusk shells, wood, bamboo, plant leaves, spider and silkworm silk (Mayer, 2005; Zhao et al., 2005, 2007; Gao, 2006; Barthelat, 2007; Fratzl and Weinkamer, 2007; Meyers et al., 2008; Bhushan, 2009; Luz and Mano, 2009; Li et al., 2010; Ritchie, 2011).

Nacre (or the mother-of-pearl), the pearly inner layer of many mollusk shells, is a typical example of natural structural composites and protective armors. It is composed of about 95 vol% inorganic aragonite platelets and 5 vol% thin layers of protein-rich biopolymers (Barthelat et al., 2007), in a multilayered ‘brick-and-mortar’ architecture. The ‘bricks’, aragonite platelets of thickness in the range of 0.2–0.9 μm and diameter in the range of 2–10 μm, are glued by the ‘mortar’,

\* Corresponding author. Tel.: +86 10 62772934; fax: +86 10 62781824.

E-mail address: [fengxq@tsinghua.edu.cn](mailto:fengxq@tsinghua.edu.cn) (X.-Q. Feng).

<sup>1</sup> Current address: Department of Mechanical Engineering, University of Michigan, Ann Arbor, MI 48109, USA.

nanoscale organic interlayers of 10–45 nm in thickness (Currey, 1977; Schäffer et al., 1997; Wang et al., 2001; Song et al., 2003; Lin and Meyers, 2005; Nassif et al., 2005; Barthelat and Espinosa, 2007). Experimental investigations of nacre have evidenced its outstanding mechanical properties, which endow it with a superior protective function. For example, the in-plane Young's modulus of nacre is in the range of 60–90 GPa (Currey, 1977; Jackson et al., 1988; Barthelat et al., 2007; Song et al., 2008), approaching the upper limit of the effective elastic modulus predicted by the Voigt model (Ji and Gao, 2004). The strain-hardening phenomenon of nacre under tension and shearing was also identified, accompanied with a high strength of 80–130 MPa and a large failure strain around 1.0% (Currey, 1977; Jackson et al., 1988; Barthelat and Espinosa, 2007), which are somewhat astonishing for such a hard and stiff material. Three- and four-point bending tests showed that the fracture toughness of nacre reaches up to 20–30 times that of pure aragonite, whose fracture toughness is about  $0.25 \text{ MPa m}^{1/2}$  (Jackson et al., 1988; Kamat et al., 2000; Barthelat et al., 2007; Tang et al., 2007). Moreover, the measured crack resistance curves (*R*-curves) (Barthelat and Espinosa, 2007; Rabiei et al., 2010) indicate a significant toughening effect with crack propagation in many types of nacles, which is very intriguing when considering the brittleness and high volume percentage of the aragonite phase in the material. Owing to its superior structural robustness, high Young's modulus and fracture toughness, nacre has attracted a great deal of interest over the past decades from scientists of materials science, solid mechanics, and biology (Barthelat, 2007). In general, the spatial arrangement and the aspect ratio of mineral platelets vary for the nacles of diverse mollusk species, which exhibit a span of mechanical properties (Fleischli et al., 2008; Rabiei et al., 2010). Some previous experimental efforts have also specifically addressed the effect of the aspect ratio of platelets (Jackson et al., 1988; Fleischli et al., 2008; Bekah et al., 2011). It is believed that the special composition and hierarchical microstructure of nacre, especially its deceptively simple stacking arrangement of hard and soft components, is of great importance to its excellent mechanical properties (Currey, 1977). To date, however, the composition-structure-property-function relations of this type of biological materials are still elusive.

There exist a number of stiffening and toughening mechanisms at different length scales, contributing to the superior mechanical properties of nacre. Some important mechanisms include:

- (i) crack blunting and branching induced by the soft organic macromolecular phase with a spatial network structure (Lin and Meyers, 2005; Rabiei et al., 2010),
- (ii) the pullout of platelets which act as bridging elements to transfer stresses between two crack faces (Jackson et al., 1988; Mayer and Sarikaya, 2002; Mayer, 2005; Barthelat and Espinosa, 2007; Rabiei et al., 2010),
- (iii) the nucleation and evolution of microcracks or microvoids around the crack tip, which play a shielding role to the remote load (Mayer, 2005; Barthelat et al., 2007; Espinosa et al., 2009),
- (iv) the bridging effect of organic ligaments which transfer tractions during the relative sliding between neighboring platelets (Jackson et al., 1988; Smith et al., 1999; Barthelat and Espinosa, 2007),
- (v) the hierarchical unfolding process of biological macromolecules and the viscoplastic energy dissipation in the fracture process zone (whitening zone) around the crack tip, which dissipate a considerable amount of applied energy (Mayer, 2005; Barthelat et al., 2007; Barthelat and Rabiei, 2011), and
- (vi) various strengthening mechanisms at the interface between neighboring layers, e.g., mineral bridges across organic layers (Song and Bai, 2003; Song et al., 2003) and nanoasperities and wavy patterns on the surfaces of platelets (Wang et al., 2001; Evans et al., 2001; Barthelat and Espinosa, 2007; Barthelat et al., 2007; Espinosa et al., 2011).

Fig. 1 schematizes some experimentally identified toughening mechanisms around the tip of a propagating crack in nacre. Most fracture experimental observations show that the crack usually goes around the platelets and occasionally through them, indicating that most platelets connecting two crack faces are pulled out from the protein-rich matrix and few are broken (Currey, 1977; Barthelat and Espinosa, 2007). These platelets serve as bridges to transfer tractions between the two crack faces, and the bridging effect of platelets has been demonstrated as the most significant mechanism for the outstanding tensile strength and fracture toughness of nacre (Jackson et al., 1988). The tensile stress transferred by a

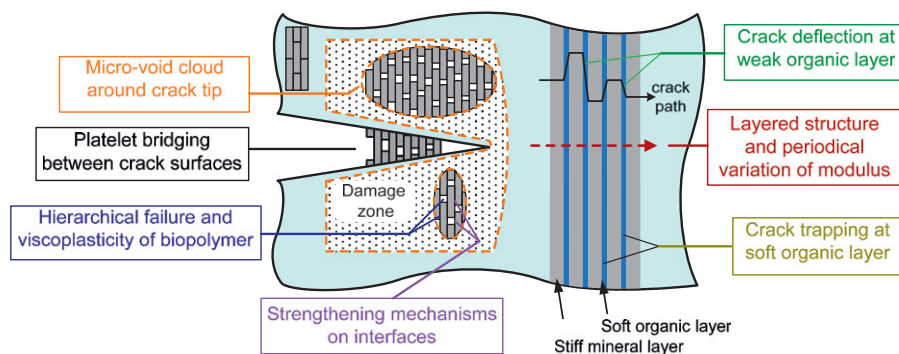


Fig. 1. Schematic of some toughening mechanisms in nacre.

platelet and the corresponding maximum energy dissipation in the bridging zone depend on such factors as the visco-elastoplastic properties of the organic phase, the geometric size and shape of the platelets, and the distribution of mineral bridges interconnecting platelets. In other words, many microscopic physical mechanisms listed above contribute to the high fracture toughness of nacre by altering the distribution of stress and energy dissipation in the crack-bridging zone of platelets. Therefore, exploring the bridging mechanism from the viewpoint of micromechanics is of particular interest for gaining a deep understanding of the superior mechanical properties of nacre, and bone as well.

Considerable attention has been paid to the theoretical modeling of the remarkable mechanical properties of nacre, particularly its tensile strength and fracture toughness. For example, Okumura and de Gennes (2001) proposed the concept of coarse-grained elastic energy to address an edge crack in a nacre-like plate. It is found that the stratified microstructure of nacre is an important factor in toughening (Okumura, 2002, 2003). Fratzl et al. (2007) applied the  $J$ -integral approach to a material with Young's modulus varying periodically. They showed that an effective crack stopping occurs when the ratio between the Young's moduli of the stiff and soft layers is larger than a critical value of about 5.0, which does not depend much on the thickness of soft layers. In other words, a very small fraction of the soft organic phase is sufficient for arresting cracks. Gao and coworkers (Gao and Ji, 2003; Gao et al., 2003; Ji and Gao, 2004; Gao, 2006) established the tension–shear chain (TSC) model to capture the prominent load transfer feature in nacre. They combined the TSC model and the Dugdale-type cohesive zone model to interpret the high fracture toughness of such biocomposites as nacre and bone. They clarified the significant roles which the nanoscale size of platelets, the hierarchical structure and the staggered platelet distribution play in the excellent mechanical behavior of this kind of biological materials (Gao et al., 2003; Gao, 2006; Zhang et al., 2010, 2011). Using the concept of continuous damage random thresholds fuse network, Nukala and Šimunović (2005) developed a simple discrete lattice model to investigate the fracture properties of nacre. They showed that the high fracture toughness of nacre results from its unique architecture, repeated unfolding of macromolecules in the organic phase, and the presence of the bundle of mineral bridges between aragonite platelets. To the best of our knowledge, however, how the microscopic mechanisms described above contribute to the superior mechanical properties of nacre is still an issue under debate, and it is of interest to establish a fracture mechanics model that can quantitatively correlate its toughness with microstructural parameters. Very recently, Barthelat and Rabiei (2011) reported their theoretical modeling of the toughness magnification in biological nanocomposites. By resorting to the  $J$ -integral method, some analytical results about the fracture toughness of materials with nacre-like microstructure were obtained. They demonstrated several important features that contribute to a high toughness, especially a process zone parameter that dictates the difference between steady-state and non-steady-state crack propagation and thus the available fracture toughness. In addition, they analyzed the effect of platelet pullout mechanism on the mechanical properties of nacre.

In addition, biomimetic materials science has become a rapidly developing field with the aim to design and fabricate novel materials using inspirations from nature (e.g., see recent review article by Ji and Gao, 2010; Ritchie, 2011). Some early attempts in synthesizing layered nacre-like toughened ceramics have been reviewed by Chan (1997). In the past decade, some state-of-the-art technologies have been developed, enabling better mimicking of nacre. For example, the organization of poly(vinyl alcohol)/montmorillonite composites treated with glutaraldehyde was prepared from the structure of nacre and this type of polymer nanocomposites has superior stiffness and strength one order of magnitude higher than those of analogous nanocomposites (Podsiadlo et al., 2007). Munch et al. (2008), Launey and Ritchie (2009) and Launey et al. (2009, 2010) developed a suite of ceramic-based hybrid bulk materials with unique hierarchical structures, which have a fracture toughness of about 30 MPa m<sup>1/2</sup> and tensile strength of about 200 MPa. Recently, effort has also been made to synthesize artificial materials mimicking the surface waviness and dovetail structure of platelets in natural nacre (Barthelat, 2010; Barthelat and Zhu, 2011; Espinosa et al., 2011). In spite of these developments, few biomimetic materials have achieved mechanical properties as good as such natural biological materials as nacre and bone because of technological restrictions and unclear understanding of the underlying toughening mechanisms and design principles of nacre. Most previous designs of biomimetic materials are only empirical duplications of natural nacre. Higher tensile strength and Young's modulus are relatively easy to achieve for artificial materials, but a simultaneous replication of a high fracture toughness and other functions seems to be difficult. Therefore, a deeper understanding of the dependence of the astonishing fracture toughness of nacre on its hierarchical structures will be helpful for optimal design and fabrication of novel biomimetic materials.

In the present paper, we establish a microstructure-based fracture mechanics model to investigate the toughening mechanisms in nacre. This paper is outlined as follows. Following this brief review of literature, we will present the fracture mechanics model to calculate the fracture toughness of nacre by accounting for the discontinuous crack-bridging mechanism of platelets of finite sizes in Section 2. The effects of such factors as the characteristic sizes and the aspect ratio of platelets, the effective Young's modulus of nacre, and the interfacial properties are examined in detail in Section 3. In this study, our particular attention is paid to the toughening effect of the crack-bridging mechanism of platelets since, as described above, it makes the most significant contribution to the high fracture toughness of nacre and some other mechanisms (e.g., the viscoplastic energy dissipation and the hierarchical unfolding mechanism enhanced by proper water content in biopolymers, and the interfacial strengthening structures) can also be reflected in this model by modulating the interfacial properties. Our study shows that the characteristic sizes and the aspect ratio of platelets observed in natural nacre are in an optimal range that leads to a combination of superior strength, stiffness and fracture toughness. An upper bound and a lower bound are derived for the average thickness of platelets to achieve a strong and reliable toughening effect.

## 2. Discontinuous crack-bridging model

### 2.1. Modeling of platelet bridging

In this section, we present a microstructure-based fracture mechanics model to correlate the fracture toughness with the structural parameters of nacre. Consider an idealized ‘brick-and-mortar’ microstructure of nacre consisting of stiff platelets (mineral phase) and soft interlayers (organic macromolecular phase), as shown in Fig. 2. Assume a crack perpendicular to the longitudinal direction of the platelets, with the crack length much larger than the thickness of platelets such that we consider it to be semi-infinite. To quantify the contribution of the crack-bridging mechanism to the macroscopic fracture toughness of nacre, a virtual configuration where no platelet has been pulled out from the crack faces is chosen as the reference state. Refer to a Cartesian coordinate system ( $O-xy$ ), where the origin  $O$  is located at the real or physical crack tip, the  $x$  and  $y$  axes are parallel and perpendicular to the crack plane, respectively. In the remote field, a uniform tensile stress is applied along the  $y$  direction (Fig. 2). Such a mode-I crack problem is of particular interest, and most experimentally measured values of the fracture toughness of nacre correspond to this symmetric crack configuration. For the sake of simplicity, the plane-strain conditions in the  $x$ - $y$  plane are assumed since the average diameter of platelets is much larger than their thickness.

For the analysis of fracture toughness of such a microstructured material, one should first define the critical initiation state of crack propagation. Experimental observations (Song et al., 2003; Barthelat and Espinosa, 2007) showed that with the increase of the externally applied load, microvoids will be formed first in the originally intact organic phase ahead of the initial crack tip (point  $O$  in Fig. 2(a)). The formation of a microvoid in the front of the crack tip indicates the pullout of a platelet. Further increasing the applied load will render distributed damage or a microvoid cloud around the crack tip, as shown in Fig. 1. In the present study, however, our attention will be focused mainly on the crack-bridging toughening mechanism of platelets. The microvoid cloud plays a shielding effect on the crack tip stress, and its contribution to fracture toughness can be estimated by using methods such as the path-independent  $J$ -integral (e.g., Hutchinson, 1987) but will be omitted in this work for simplicity.

To rationalize the toughening effect of crack-bridging by platelets, it is essential to choose a fracture criterion in terms of an appropriate mechanical parameter. As is frequently referred to in the classical Dugdale–Barenblatt model and most cohesive zone models for conventional composites reinforced by fibers or whiskers (McMeeking and Evans, 1982; Mai and Lawn, 1987; Budiansky and Amazigo, 1989; Evans, 1990), we use the stress intensity factor (SIF) at the crack tip as the parameter to judge the occurrence of crack propagation. Let  $K_I^\infty$  designate the SIF at the crack tip  $O$  caused by the remote stress. In the reference configuration without any platelet having been pulled out, a microvoid will appear in the thin

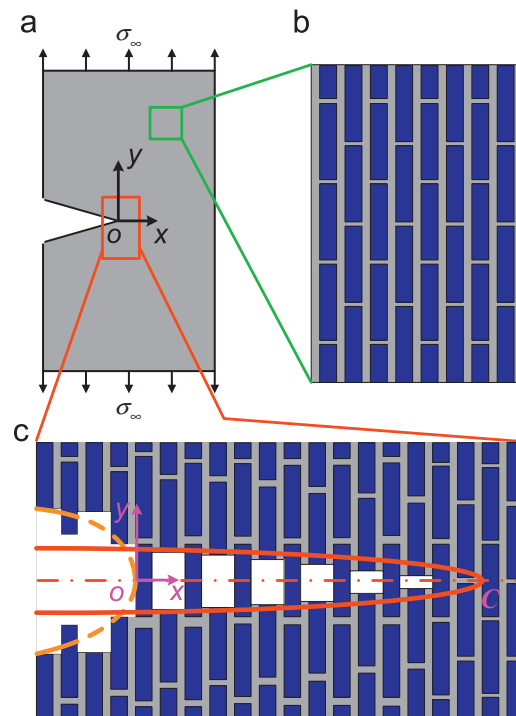


**Fig. 2.** (a) Schematic of a mode-I crack configuration in nacre. (b) A typical brick-and-mortar stacking pattern of platelets. (c) Schematic of a crack with discrete platelet bridging in nacre.

organic layer just ahead of the crack tip  $O$  when the external load reaches a critical value, which indicates the pullout of the first platelet. At this moment, it is obvious that the SIF caused by the remote stress must equal to the intrinsic toughness of nacre,  $K_I^0$ , which accounts for the toughness without the toughening effect of any crack-bridging platelet, that is,

$$K_I^\infty = K_I^0. \tag{1}$$

Here, it is of importance to have a brief discussion on  $K_I^0$ , which is taken as a material constant reflecting the energy dissipated by the breakage of organics to form a void ahead of the crack tip. Since the value of  $K_I^0$  is difficult to be measured experimentally, we can only give our best estimation here. As an approximation, the normal stress in the platelet nearest to the crack tip is given as  $K_I^0/\sqrt{\pi d}$ , where the platelet thickness  $d$  is of the order of 100 nm. On the other hand, the yield strength of the aragonite platelet is measured by nanoindentation tests to be of the order of 1 GPa (Bruet et al., 2005; Barthelat et al., 2006). Under the concept of maximal utilization of the structural elements (Gao et al., 2003; Fleischli et al., 2008), the normal stress in the platelet and its strength should be of the same order when there is no high stress concentration (Bekah et al., 2011). This indicates that  $K_I^0$  can be of the order of 1 MPa m<sup>1/2</sup>. Therefore, we set  $K_I^0 = 1 \text{ MPa m}^{1/2}$  in this study.

Under an increasing applied stress, more and more platelets will be pulled out and form bridges between the two crack surfaces, leading to an extension of the crack-bridging zone. In the discontinuous crack-bridging model presented here, the left and right ends of the crack-bridging zone in Fig. 2(c) are referred to as the physical or real crack tip and the fictitious crack tip, respectively. Though fracture toughness can vary locally in inhomogeneous materials, especially at the interface between materials with different mechanical properties, for the sake of simplicity, the material outside the bridging zone is treated as a homogeneous, isotropic, and linear elastic medium by invoking the homogenization technique in micromechanics. The effect of anisotropy on the pure mode-I SIF in Fig. 2 can be easily taken into account by using the methods described by Tada et al. (1985) and Budiansky and Amazigo (1989), but is neglected in this study. The value of the effective Young’s modulus  $E$  is approximately taken to be the experimentally measured in-plane stiffness in uniaxial tension tests. Thereafter, a two-dimensional crack-bridging model considering the microstructural features of nacre is shown in Fig. 3(a). In this model, the bridging forces induced by the platelets within the crack-bridging zone are reasonably treated as a series of discrete concentrated forces, as shown in Fig. 3(b), given the fact that the platelet has a much larger thickness than the organic layer. A similar discretization method of bridging forces was recently adopted by Barthelat and Rabiei (2011).

When the remote stress increases to a threshold value, the semi-infinite crack will enter a steady-state propagation, in which the crack propagates but the crack-bridging zone is kept at a constant length. In this situation, a new platelet bridge formed at the right end of the crack-bridging zone is always accompanied by a complete pullout of a platelet at the left end.

From the initiation to the steady state of the bridging zone, the following critical condition of SIFs should be satisfied

$$K_I^\infty + K_I^{\text{br}} = K_I^0, \tag{2}$$

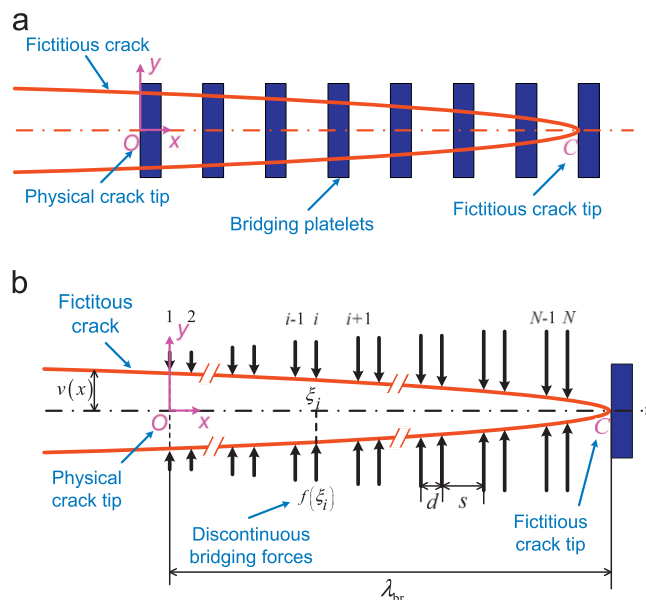


Fig. 3. Discontinuous crack-bridging model of nacre. (a) A number of platelets are pulled out, forming a bridging zone behind the crack tip, C. (b) The traction in the crack-bridging zone are discretized into a series of concentrated forces  $f(\xi_i)$ .

where  $K_1^{\text{br}}$  denotes the reduction of SIF caused by the bridging forces and thus has a negative value. It is emphasized that the SIF  $K_1^\infty$  characterizes the actual fracture toughness of the material and corresponds to the measured results in most experiments, while  $K_1^{\text{br}}$  only represents the part of  $K_1^\infty$  that comes from the crack-bridging toughening mechanism of platelets.

The contribution of the crack-bridging zone to the fracture toughness,  $K_1^{\text{br}}$ , can be calculated by (Budiansky and Amazigo, 1989; Broberg, 1999)

$$K_1^{\text{br}} = -\sqrt{\frac{2}{\pi}} \int_0^{\lambda_{\text{br}}} \frac{\sigma_{\text{br}}(x)}{\sqrt{\lambda_{\text{br}}-x}} dx, \quad (3)$$

where  $\sigma_{\text{br}}(x)$  is the bridging traction and  $\lambda_{\text{br}}$  is the length of the crack-bridging zone, which follows the geometric condition:

$$\lambda_{\text{br}} = N(d + d_{\text{int}}), \quad (4)$$

$d$  and  $d_{\text{int}}$  are the thicknesses of platelets and interfacial layers, respectively, and  $N$  is the number of the discrete bridging forces or twice the number of platelets in the crack-bridging zone. Eq. (3) has often been used to predict the fracture toughness of fiber-reinforced composites (Budiansky and Amazigo, 1989), and we inherit its validity in this study. As aforementioned, the bridging traction is here treated as a series of concentrated forces  $f(\xi_i)$  by considering the actual load transfer features of platelets. Here,  $\xi_i$  present the locations where these forces act and are given by

$$\xi_i = \begin{cases} (i-1)(d + d_{\text{int}}), & \text{when } i \text{ is odd,} \\ [(i-1)d + (i-2)d_{\text{int}}], & \text{when } i \text{ is even.} \end{cases} \quad (5)$$

Herein and in the sequel, the index  $i$  takes the integers from 1 to  $N$ . The bridging force  $f(\xi_i)$  is determined by the relation

$$f(\xi_i) = \tau(\xi_i) \left[ \frac{l}{2} - v(\xi_i) \right], \quad (6)$$

where  $l$  is the length of the platelet.  $v(\xi_i)$  is the crack face opening displacement at the position  $x = \xi_i$  and equals to the pullout length of the platelet at the same location.  $\tau(\xi_i)$  is the average shear stress in the biopolymer interlayer, applied on the interface between the bridging platelet and the organic matrix. It is reasonable to assume that  $\tau(\xi_i)$  is a function of the relative sliding displacement between two neighboring platelets, i.e.,  $v(\xi_i)$ , that is,

$$\tau(\xi_i) = \tau(v(\xi_i)). \quad (7)$$

Its expression will be given in Section 2.2.

Thus the tensile stress acting on the two crack faces in the crack-bridging zone can be expressed as

$$\sigma_{\text{br}}(\xi) = \sum_{i=1}^N [f(\xi) \delta(\xi - \xi_i)], \quad (8)$$

where  $\delta(\xi - \xi_i)$  is the Dirac's delta function centered at  $\xi = \xi_i$ .

From Eqs. (3)–(8), the toughening effect due to the platelet bridging mechanism is recast as

$$K_1^{\text{br}} = -\sqrt{\frac{2}{\pi}} \sum_{i=1}^N \frac{\tau(\xi_i)}{\sqrt{\lambda_{\text{br}} - \xi_i}} \left[ \frac{l}{2} - v(\xi_i) \right]. \quad (9)$$

The above model allows one not only to rationalize the dependence of the fracture toughness on the microstructural parameters of nacre but also to examine the effects of the thickness and aspect ratio of platelets, the mechanical properties of the organic phase, and some other factors (e.g., temperature and water content), as will be discussed below.

## 2.2. Interfacial cohesive law

For the use of the crack-bridging model, one needs to determine the force exerted on a bridging platelet in the cohesive zone as a function of its pullout length or the crack opening displacement. Direct determination of this force-displacement relation is a challenging issue because there exist a number of factors that can influence the mechanical properties of the interface between the organic and the mineral phase, e.g., the interfacial layer thickness, water content, surface waviness of platelets, and mineral bridges between neighboring platelets. For the simplicity of mathematical manipulation, we assume that the curve determining the relation between the shear stress  $\tau(\xi_i)$  and the relative sliding displacement  $v(\xi_i)$  has a trapezoidal-like shape (Barthelat et al., 2007), as shown in Fig. 4, characterized by a stress plateau during platelet pullout following the elastic deformation stage and ending with interfacial softening as the interlayer fails. The interfacial cohesive law is expressed as

$$\tau = \begin{cases} \frac{v}{\delta_1} \tau_{\text{max}} & 0 \leq v \leq \delta_1, \\ \tau_{\text{max}} & \delta_1 \leq v \leq \delta_2, \\ \frac{\delta_c - v}{\delta_c - \delta_2} \tau_{\text{max}} & \delta_2 \leq v \leq \delta_c, \end{cases} \quad (10)$$

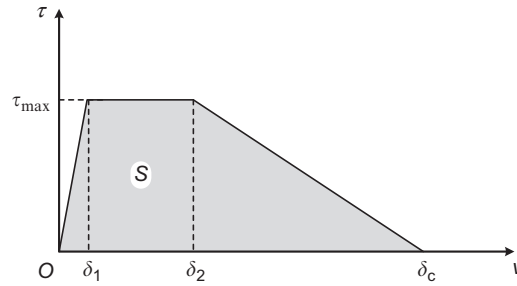


Fig. 4. Trapezoidal interfacial cohesive law.

where  $\tau_{\max}$  is the interfacial strength,  $\delta_1$ ,  $\delta_2$  and  $\delta_c$  are material constants. In Eq. (10),  $\delta_c$  stands for the ultimate pullout length of a platelet, and we denote  $\delta_c = \delta_c^{\text{eff}} \cdot l$ , with  $\delta_c^{\text{eff}}$  being a dimensionless critical pullout length with respect to the platelet length. The energy dissipated by the interfacial layer per unit area during the pullout process, i.e., the separation work  $S$ , is determined by the area of the trapezoid in Fig. 4 as (Tvergaard and Hutchinson, 1992)

$$S = \int_0^{\delta_c} \tau d\delta = \frac{1}{2} \tau_{\max} [\delta_c + \delta_2 - \delta_1]. \quad (11)$$

Although the constitutive relation in Eq. (10) has four parameters ( $\tau_{\max}$ ,  $\delta_1$ ,  $\delta_2$ , and  $\delta_c$ ), the adhesive property of the organic–inorganic interfaces is usually characterized by two key parameters, namely the maximal shear stress  $\tau_{\max}$  and the separation work  $S$  (Tvergaard and Hutchinson, 1992; Barthelat et al., 2007). This simplified interfacial cohesive model can capture the prominent features of the dependence of the interfacial shear stress on the relative sliding displacement between two neighboring platelets and has been extensively employed in the simulations of adhesive contact, interface delamination, peel test, and many other problems (Tvergaard and Hutchinson, 1993; Wei and Hutchinson, 1998; Lu et al., 2007; Li et al., 2012). More complicated adhesion models, e.g., the Lennard–Jones potential adopted by Cho and Park (2004), can also be implemented easily into the present crack-bridging model, but they often need more parameters and more complicated calculations. The influence of the assumed trapezoidal shape of the interfacial cohesive law will be examined in detail by numerical examples in Section 3.3.

### 2.3. Calculation of crack opening displacement

To determine the crack-bridging forces of individual platelets at positions  $\xi_i$ , one should calculate the crack opening displacements,  $v(\xi_i)$ , at these positions. The crack opening displacement of a semi-infinite crack subjected to the SIF caused by the remote stress,  $K_1^\infty$ , and the bridging traction  $\sigma_{\text{br}}(\xi)$  is expressed as (Broberg, 1999)

$$v(x) = \frac{4K_1^\infty \sqrt{\lambda_{\text{br}} - x}}{\sqrt{2\pi E}} - \frac{2}{\pi E} P.V. \int_0^{\lambda_{\text{br}}} \ln \frac{\sqrt{\lambda_{\text{br}} - x} + \sqrt{\lambda_{\text{br}} - \xi}}{\sqrt{\lambda_{\text{br}} - x} - \sqrt{\lambda_{\text{br}} - \xi}} \sigma_{\text{br}}(\xi) d\xi, \quad (12)$$

where  $P.V.$  presents the Cauchy principal value of the integral, and  $E$  is the effective modulus of nacre. From Eqs. (3)–(8) and (12), the crack opening displacement induced by the discontinuous crack-bridging platelets can be rewritten as

$$v(x) = \frac{4K_1^\infty \sqrt{\lambda_{\text{br}} - x}}{\sqrt{2\pi E}} - \frac{2}{\pi E} p.v. \sum_{n=1}^N \ln \frac{\sqrt{\lambda_{\text{br}} - x} + \sqrt{\lambda_{\text{br}} - \xi_n}}{\sqrt{\lambda_{\text{br}} - x} - \sqrt{\lambda_{\text{br}} - \xi_n}} \tau(\xi_n) \left[ \frac{l}{2} - v(\xi_n) \right], \quad (13)$$

where  $p.v.$  is the discretized form of  $P.V.$  The detailed expression of  $p.v.$  is given in Appendix A. It is worth mentioning that Eq. (12) holds for a crack in an isotropic, linear elastic and infinite body, and the effects of anisotropy and inelastic deformation have not been accounted for in this study.

Using Eqs. (2) and (9), the crack opening displacement in Eq. (13) is reformulated in terms of the intrinsic toughness  $K_1^0$  as

$$v(x) = \frac{4K_1^0 \sqrt{\lambda_{\text{br}} - x}}{\sqrt{2\pi E}} + \frac{4\sqrt{\lambda_{\text{br}} - x}}{\pi E} \sum_{n=1}^N \frac{\tau(\xi_n)}{\sqrt{\lambda_{\text{br}} - \xi_n}} \left[ \frac{l}{2} - v(\xi_n) \right] - \frac{2}{\pi E} p.v. \sum_{n=1}^N \ln \frac{\sqrt{\lambda_{\text{br}} - x} + \sqrt{\lambda_{\text{br}} - \xi_n}}{\sqrt{\lambda_{\text{br}} - x} - \sqrt{\lambda_{\text{br}} - \xi_n}} \tau(\xi_n) \left[ \frac{l}{2} - v(\xi_n) \right]. \quad (14)$$

Then letting  $x = \xi_i$  in Eq. (14), we obtain a system of  $N$  discretized equations for the crack opening displacements in the crack-bridging zone:

$$v(\xi_i) = \frac{4K_1^0 \sqrt{\lambda_{\text{br}} - \xi_i}}{\sqrt{2\pi E}} + \frac{4\sqrt{\lambda_{\text{br}} - \xi_i}}{\pi E} \sum_{n=1}^N \frac{\tau(\xi_n)}{\sqrt{\lambda_{\text{br}} - \xi_n}} \left[ \frac{l}{2} - v(\xi_n) \right] - \frac{2}{\pi E} p.v. \sum_{n=1}^N \ln \frac{\sqrt{\lambda_{\text{br}} - \xi_i} + \sqrt{\lambda_{\text{br}} - \xi_n}}{\sqrt{\lambda_{\text{br}} - \xi_i} - \sqrt{\lambda_{\text{br}} - \xi_n}} \tau(\xi_n) \left[ \frac{l}{2} - v(\xi_n) \right], \quad (15)$$

with  $i=1,2,\dots,N$ . Obviously, the function  $v(\xi_i)$  monotonically increases with respect to  $\xi_i$ , and  $0 < v(\xi_i) < \delta_c$  should be satisfied for all effective bridging platelets. In the solution of Eq. (15), the value of  $N$  is set one at a time, in order to reflect the

extension of bridging zone. With each  $N$ , a numerical iteration method is employed to solve for the corresponding displacements  $v(\xi_i)$  in Eq. (15). The calculation will be terminated when the solution reaches  $v(\xi_1) \geq \delta_c$ , which indicates a saturated bridging zone and thus the maximal bridging toughening effect.

Introduce the following dimensionless parameters,

$$\begin{aligned} v^*(x) &= \frac{v(x)}{d_{\text{int}}}, & E^* &= \frac{E\sqrt{d_{\text{int}}}}{4K_1^0}, & N &= \frac{\lambda_{\text{br}}}{d+d_{\text{int}}}, \\ d^* &= \frac{d}{d_{\text{int}}}, & l^* &= \frac{l}{d_{\text{int}}}, & \tau^*(\xi_n) &= \frac{\tau(\xi_n)\sqrt{d_{\text{int}}}}{K_1^0}, \end{aligned} \quad (16)$$

the crack surface displacement in Eq. (15) becomes

$$v^*(\xi_i) = \frac{\sqrt{\lambda_{\text{br}} - \xi_i}}{E^* \sqrt{2\pi d_{\text{int}}}} + \frac{1}{\pi E^*} \sum_{n=1}^N \frac{\sqrt{\lambda_{\text{br}} - \xi_i}}{\sqrt{\lambda_{\text{br}} - \xi_n}} \tau^*(\xi_n) \left[ \frac{l^*}{2} - v^*(\xi_n) \right] - \frac{1}{2\pi E^*} p \cdot v \cdot \sum_{n=1}^N \ln \frac{\sqrt{\lambda_{\text{br}} - \xi_i} + \sqrt{\lambda_{\text{br}} - \xi_n}}{\sqrt{\lambda_{\text{br}} - \xi_i} - \sqrt{\lambda_{\text{br}} - \xi_n}} \tau^*(\xi_n) \left[ \frac{l^*}{2} - v^*(\xi_n) \right]. \quad (17)$$

For simplicity, the interfacial cohesive law in Eq. (10) can be recast into a dimensionless form as

$$\tau^* = \begin{cases} \frac{l^*}{\delta_1^*} \tau_{\text{max}}^* & 0 \leq v^* \leq \delta_1^*, \\ \tau_{\text{max}}^* & \delta_1^* \leq v^* \leq \delta_2^*, \\ \frac{\delta_c^* - v^*}{\delta_c^* - \delta_2^*} \tau_{\text{max}}^* & \delta_2^* \leq v^* \leq \delta_c^*, \end{cases} \quad (18)$$

where the corresponding dimensionless parameters are defined as

$$\tau_{\text{max}}^* = \frac{\tau_{\text{max}} \sqrt{d_{\text{int}}}}{K_1^0}, \quad \delta_1^* = \frac{\delta_1}{d_{\text{int}}}, \quad \delta_2^* = \frac{\delta_2}{d_{\text{int}}}, \quad \delta_c^* = \frac{\delta_c}{d_{\text{int}}}. \quad (19)$$

In addition, it is required that the tensile stress in each platelet in the crack-bridging zone must be lower than the tensile strength of the mineral phase,  $\sigma_{\text{max}}^{\text{aragonite}}$ , that is,

$$\max_{i=1,2,\dots,N} \left\{ \tau(\xi_i) \left[ \frac{l}{2} - v(\xi_i) \right] \right\} < \frac{1}{2} d \cdot \sigma_{\text{max}}^{\text{aragonite}}, \quad (20)$$

whose dimensionless form is

$$\max_{i=1,2,\dots,N} \left\{ \tau^*(\xi_i) \left[ \frac{l^*}{2} - v^*(\xi_i) \right] \right\} < \frac{d}{d_{\text{int}}} \frac{\sigma_{\text{max}}^{\text{aragonite}} \sqrt{d_{\text{int}}}}{2K_1^0} = \frac{1}{2} d^* \sigma_{\text{max}}^* \sigma_{\text{max}}^{\text{aragonite}}. \quad (21)$$

Near the crack tip, the crack opening displacement  $v^*(\xi_i)$  is usually very small in comparison with platelet length, and the magnitude of  $\tau^*(v^*(\xi_i))$  is of the same order of  $\tau_{\text{max}}^*$ . Therefore, the left side of Eq. (21) can be approximated as  $l^*/2 - v^*(\xi_i) \approx l^*/2$  and  $\tau^*(v^*(\xi_i)) \approx \tau_{\text{max}}^*$ , and Eq. (21) reduces to

$$\frac{l^*}{d^*} < \frac{\sigma_{\text{max}}^* \sigma_{\text{max}}^{\text{aragonite}}}{\tau_{\text{max}}^*}. \quad (22)$$

This condition finds its root in the concept of optimum aspect ratio of platelets (Gao et al., 2003) and the stress analysis of platelets under tension (Bekah et al., 2011).

#### 2.4. Toughening ratio

As aforementioned, when the remote stress reaches a threshold value, the semi-infinite crack will propagate in a steady manner. In this stage, the length of the bridging zone will remain constant, designated as  $\lambda_{\text{br}}^{\text{SS}}$ , rendering an invariant toughening effect. From Eqs. (9), (16)–(19), the crack opening displacements and the tensile stresses in all platelets in the bridging zone can be solved at any state from the initial propagation of the crack to the saturation of the bridging zone. Thus, one can obtain the SIF at the crack tip due to the external applied load,  $K_1^\infty$ , and the SIF reduction due to the crack-bridging effect of platelets,  $K_1^{\text{br}}$ . Then the toughening ratio  $\eta$  can be determined as

$$\eta = \left| \frac{K_1^{\text{br}}}{K_1^0} \right| = \sqrt{\frac{2}{\pi}} \sum_{n=1}^N \frac{\sqrt{d_{\text{int}}}}{\sqrt{\lambda_{\text{br}} - \xi_n}} \tau^*(\xi_n) \left[ \frac{l^*}{2} - v^*(\xi_n) \right], \quad (23)$$

which quantifies the toughening effect of the crack-bridging mechanism of platelets.

In engineering practice, the fracture toughness at the stage of steady-state crack propagation is always of particular interest. Therefore, we define the steady-state toughening ratio,  $\eta_{\text{SS}}$ , by

$$\eta_{\text{SS}} = \left| \frac{K_1^{\text{br}}}{K_1^0} \right| = \sqrt{\frac{2}{\pi}} \sum_{n=1}^N \frac{\sqrt{d_{\text{int}}}}{\sqrt{\lambda_{\text{br}}^{\text{SS}} - \xi_n}} \tau^*(\xi_n) \left[ \frac{l^*}{2} - v^*(\xi_n) \right], \quad (24)$$

which reflects the maximal toughening effect the platelets can achieve. Since the steady-state length of the bridging zone,  $\lambda_{br}^{SS}$ , depends on the geometric and mechanical parameters of the microstructure of nacre,  $\eta_{SS}$  can be written as a function as

$$\eta_{SS} = \Phi(d^*, l^*, E^*, \tau_{max}^*, \delta_1^*, \delta_2^*, \delta_C^{eff}). \quad (25)$$

It is emphasized that the parameter  $\eta_{SS}$  in our model corresponds to the experimentally measured fracture toughness at the level-out point of the *R*-curve of nacre, where the bridging zone has saturated (Barthelat and Espinosa, 2007). Thus, Eqs. (16)–(19), (23) and (24) provide all equations in the discontinuous crack-bridging model for analyzing the fracture toughness of nacre.

A quantitative comparison between our theoretical results and the relevant experimental measurements will be given in Section 3.1.

### 3. Results and discussions

#### 3.1. Effect of the size and aspect ratio of platelets

In this section, we first examine how the toughening effect of the crack-bridging mechanism of platelets depends on their characteristic sizes. First, the toughening ratio  $\eta$ , the steady-state bridging zone length  $\lambda_{br}^{SS}$ , and the steady-state toughening ratio  $\eta_{SS}$  are shown in Fig. 5 as a function of the platelet thickness  $d$ . For several representative values of the platelet thickness in the range of 30–600 nm, Fig. 5(a) gives the curves of  $\eta$  with the increase of the crack-bridging zone length. The parameters used in our calculations are listed in Table 1.

As can be seen from Fig. 5(a), the toughening ratio  $\eta$  increases with the extension of the bridging zone until it reaches the steady-state value,  $\eta_{SS}$ . When the platelets are relatively thin (e.g.,  $d=30$  nm or 60 nm), the  $\eta$ -curve rises more and the corresponding steady-state value  $\eta_{SS}$  is high. This result demonstrates a strong size effect of the toughening mechanism: the thinner the platelets, the higher the fracture toughness. In addition, the steady-state length of the bridging zone,  $\lambda_{br}^{SS}$ , is approximately proportional to the thickness of platelets, as shown in Fig. 5(b). Therefore, thinner platelets can more efficiently enhance the resistance capacity of nacre to crack propagation and yield higher fracture toughness. This result is consistent with the experimental measurements of the fracture toughness of nacre with various platelet thicknesses (Fleischli et al., 2008).

The dependence of the steady-state toughening ratio  $\eta_{SS}$  on the normalized platelet thickness  $d^*$  is plotted in Fig. 5(c). Clearly,  $\eta_{SS}$  decreases with the increase in  $d^*$ , and a sub-micron thickness is of importance for the platelets to achieve a higher fracture toughness of nacre. However, it is counterintuitive that the toughness might increase without bound as the platelets continue thinning down. A lower limit for the platelet thickness is determined by our model to be about 30 nm, below which the platelets will be broken before they are pulled out because of the high tensile stress in them. Thus the bridging effect will be greatly compromised when the platelets are thinner than such a lower limit. This critical thickness predicted by our model is close to the critical characteristic size determined by Gao et al. (2003) based on the concept of flaw tolerance. The above results show that the fracture toughness of nacre exhibits a significant size dependence on the platelet thickness, which should be in an optimal range bounded by two characteristic values we determined above in order to achieve a significant toughening effect.

The effect of the platelet length on the bridging zone length  $\lambda_{br}^{SS}$ , the toughening ratio  $\eta$ , and its steady-state value  $\eta_{SS}$  are illustrated in Fig. 6, where the parameters in Table 1 are used. We vary the platelet length in the range from 1  $\mu\text{m}$  to 10  $\mu\text{m}$ . As shown in Fig. 6(a), the length of the steady-state bridging zone increases with the length of platelets and asymptotically approaches a ceiling value. Fig. 6(b) shows the variation of the toughening ratio  $\eta$  with respect to the platelet length. It is seen that for longer platelets, the  $\eta$ -curves rise more rapidly and have a larger steady-state value  $\eta_{SS}$ , suggesting a higher fracture toughness. The value of  $\eta_{SS}$  is almost proportional to the normalized platelet length, as shown in Fig. 6(c). This suggests that a greater toughening effect can be obtained by elongating the platelets. However, our calculation also shows that the platelets should be shorter than a characteristic length in order to ensure that they will not be broken before being pulled out from the matrix. The upper bound of the platelet length is about 66  $\mu\text{m}$  when the parameters in Table 1 are used. Recently, Barthelat and Rabiei (2011) also analyzed the size effect of platelets on the toughness of nacre by using the *J*-integral method and concluded that the sizes of platelets should be minimized in order to maximize the overall toughness. In this study, we have determined not only the optimal range of the thickness of platelets but also that of their length.

According to the above analysis, a larger aspect ratio of platelets with nanosized thickness and microsized length is essential for nacre to achieve a higher fracture toughness. In Fig. 6(d), we compare the steady-state toughening ratio  $\eta_{SS}$  with respect to the normalized platelet length under several representative values of the aspect ratio  $l/d$ . A larger aspect ratio of platelets in nacre increases the pullout length of platelets during crack extension and allows the organic interfacial layers to transfer larger tensile forces without increasing the interfacial shear stress. Therefore, slender platelets with a staggering structure can endow nacre with superior stiffness and strength, in agreement with the conclusion of Ji and Gao (2004). In addition, since the overlapping or pullout length of platelets is sensitive to their staggering manner, our model can also account for the effect of the spatial distribution modes of parallel platelets, which is not discussed in the present paper.

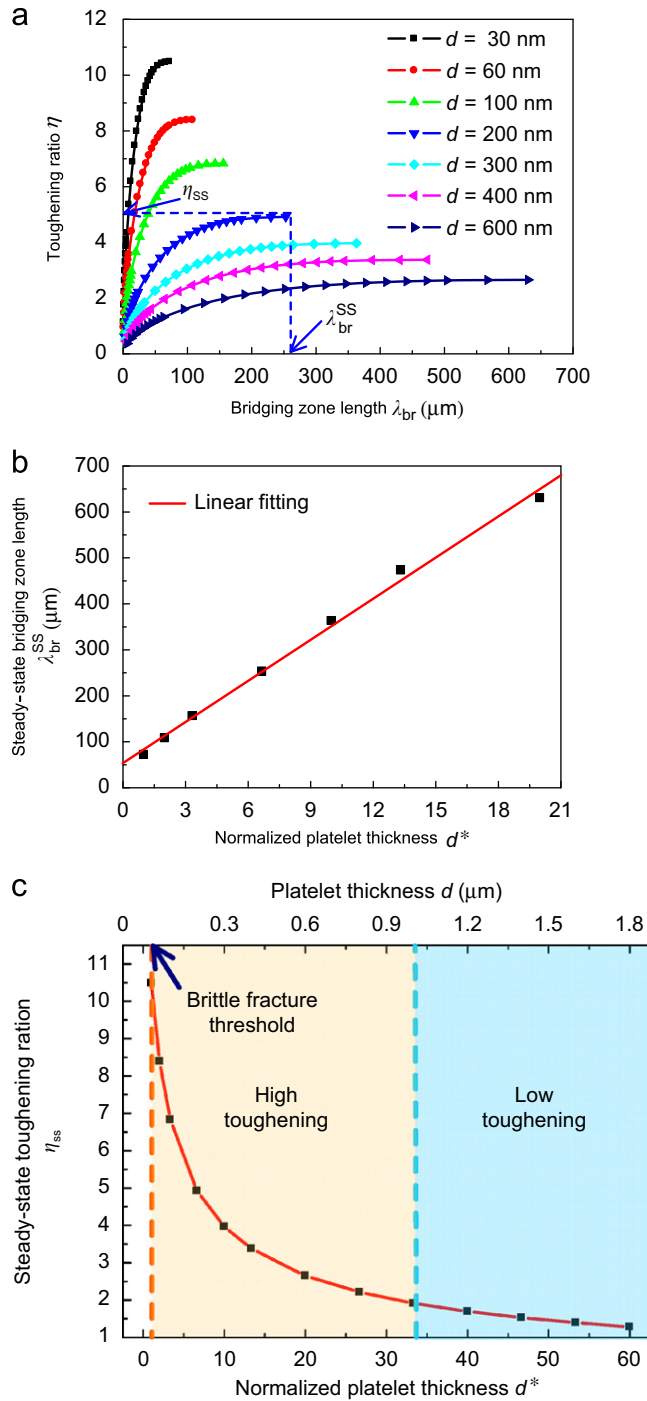


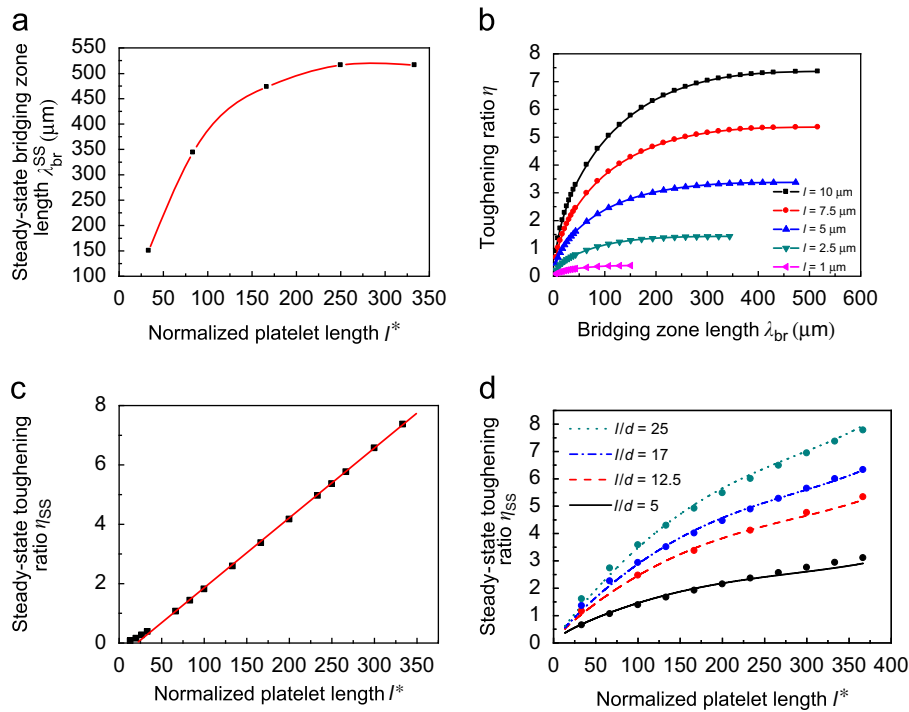
**Fig. 5.** Effects of the platelet thickness  $d$  on (a) the curve of the toughening ratio  $\eta$ , (b) the steady-state length of the bridging zone,  $\lambda_{br}^{SS}$ , and (c) the steady-state toughening ratio,  $\eta_{ss}$ . In (c), the upper and lower limits of the platelet thickness are determined from the high fracture toughness of nacre and the brittle fracture of platelets, respectively.

To further corroborate the present fracture mechanics model, we compare the theoretical fracture toughness with relevant experimental results. The steady-state toughness predicted by our model varies from  $2.7 \text{ MPa m}^{1/2}$  to  $10.5 \text{ MPa m}^{1/2}$ , corresponding to different representative values of the platelet thickness and length (Figs. 5(c) and 6(c)). Meanwhile, most experimentally measured fracture toughness of different types of nacre with various sizes of platelets is in the range from  $4 \text{ MPa m}^{1/2}$  to  $12 \text{ MPa m}^{1/2}$  (Sarikaya, 1994; Barthelat and Espinosa, 2007; Fleischli et al., 2008), which quantitatively validates our theoretical model. For example, when the platelets have a length of  $7 \mu\text{m}$  and a thickness of

**Table 1**

Parameters and their values adopted in the calculation.

Parameter	Value	References
Characteristic slipping length, $\delta_1$	5 nm	Barthelat et al. (2007); Tang et al. (2007)
Characteristic slipping length, $\delta_2$	300 nm	Barthelat et al. (2007); Tang et al. (2007)
Normalized critical pullout length, $\delta_c^{\text{eff}}$	0.44	
Interfacial shear strength, $\tau_{\text{max}}$	30 MPa	Menig et al. (2000); Barthelat et al. (2007); Lin and Meyers (2009)
Effective modulus of nacre, $E$	60 GPa	Jackson et al. (1988); Wang et al. (2001); Barthelat and Espinosa (2007)
Organic layer thickness, $d_{\text{int}}$	30 nm	Wang et al. (2001); Song et al. (2003)
Platelet length, $l$	5 $\mu\text{m}$	Song et al. (2003); Li et al. (2004); Lin and Meyers (2005)
Platelet strength, $\sigma_{\text{max}}^{\text{aragonite}}$	5 GPa	Bruet et al. (2005); Barthelat et al. (2006)
Platelet thickness, $d$	400 nm	Song et al. (2003); Li et al. (2004); Lin and Meyers (2005); Barthelat and Espinosa (2007)
Toughness without bridging, $K_I^0$	1.0 MPa m <sup>1/2</sup>	See text

**Fig. 6.** Effects of the platelet length  $l$  on (a)  $\lambda_{\text{br}}^{\text{SS}}$ , (b)  $\eta$ -curve, and (c)  $\eta_{\text{SS}}$ . (d) Effect of the aspect ratio  $l/d$  on  $\eta_{\text{SS}}$ .

400 nm, our model predicts the steady-state toughness to be 5.97 MPa m<sup>1/2</sup>, which is close to the value of 5.30 MPa m<sup>1/2</sup> measured by Barthelat and Espinosa (2007).

In addition, the above results provide some clues for optimal design of nacre-like, biomimetic composites. On one hand, to achieve a higher toughening effect, the platelets should be thinner than a critical value of a few hundred nanometers, as demonstrated by our analysis and recent experiments (Munch et al., 2008; Tang et al., 2003; Burghard et al., 2006; Bonderer et al., 2008). On the other hand, the platelets should be thicker than another critical value to ensure that they will not be broken before being pulled out from the crack surface. Thus, an optimized size range of platelets can be determined by considering their crack-bridging mechanism and tensile fracture. Furthermore, an optimal design of the overlapping distributions of platelets also allows us to improve the fracture toughness of nacreous materials. Recently, the significance of a larger aspect ratio of platelets has also found its way as a feasible strategy to achieve superior toughness and strength in novel materials mimicking the microstructure of nacre (Bonderer et al., 2008).

### 3.2. Effect of effective Young's modulus

The merger of high Young's modulus and high fracture toughness is a prominent feature of the mechanical properties of nacre. In this subsection, we will explore the influence of the effective modulus of nacre on its fracture toughness. Fig. 7 shows the effect of the effective Young's modulus  $E$  on the toughening ratio  $\eta$ , the bridging zone length  $\lambda_{\text{br}}^{\text{SS}}$ , and the steady-state toughening ratio  $\eta_{\text{SS}}$ . It is seen that the toughening ratio increases with increasing  $E$ . In other words, the stiffer

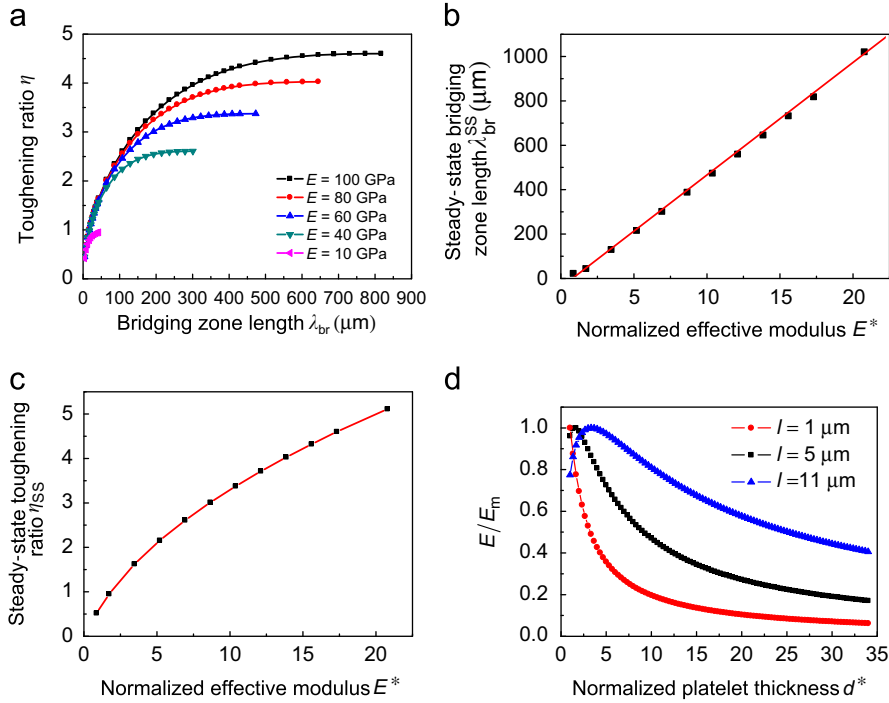


**Fig. 7.** The influence of the effective Young's modulus  $E$  on (a)  $\eta$ -curve, (b)  $\lambda_{br}^{SS}$ , and (c)  $\eta_{SS}$ . (d) The relation between platelet sizes and the effective Young's modulus of nacre.

the bulk nacre, the higher its fracture toughness, as shown in [Barthelat and Rabiei \(2011\)](#). When the bridging zone is relatively short, the  $\eta$ -curves under different values of  $E$  have little difference, as shown in [Fig. 7\(a\)](#). [Fig. 7\(b\)](#) shows that the steady-state length of the crack-bridging zone,  $\lambda_{br}^{SS}$ , increases approximately linearly with respect to the normalized Young's modulus,  $E^*$ . The steady-state toughening ratio  $\eta_{SS}$  shows a distinct dependence on  $E^*$  ([Fig. 7\(c\)](#)), and it increases rapidly with rising  $E^*$ . These results reveal the compatibility between the high stiffness and high toughness in nacre and suggest a beneficial role which the high stiffness of nacre plays in enhancing its fracture toughness. Therefore, from the perspective of structure-property relationship, the brick-and-mortar microstructure of nacre, which results from natural evolution and optimization for many millions of years, can efficiently integrate superior stiffness and fracture toughness together.

According to the TSC model of [Gao et al. \(2003\)](#), the effective Young's modulus  $E$  of nacre-like biocomposites can be calculated by

$$\frac{1}{E} = \frac{4(1-\phi)}{\mu_p \phi^2 \rho^2} + \frac{1}{\phi E_m}, \quad (26)$$

where  $\phi$  denotes the volume fraction of mineral platelets,  $\rho$  the aspect ratio of platelets,  $E_m$  the Young's modulus of platelets, and  $\mu_p = E_p/2(1+\nu_p)$  the shear modulus of the interfacial layer.  $E_p$  and  $\nu_p$  are the Young's modulus and Poisson's ratio of the organic phase, respectively. In terms of  $\phi \approx d/(d+d_{int}) = d^*/(1+d^*)$  and  $\rho = l^*/d^*$ , Eq. (26) can be rewritten as the following dimensionless form:

$$\frac{E_m}{E} = \frac{4(1+d^*)}{(l^*)^2} \cdot \frac{E_m}{\mu_p} + \frac{(1+d^*)}{d^*}. \quad (27)$$

Assuming  $\nu_p = 0.5$  and  $E_m/E_p = 1000$  ([Ji and Gao, 2004](#)), a normalized relationship between the effective Young's modulus  $E$  of nacre and the dimensionless thickness  $d^*$  of platelets is obtained from Eq. (27) and plotted in [Fig. 7\(d\)](#). It can be easily seen that in the considered range of the thickness and length of platelets, both the effective Young's modulus and fracture toughness of the material can be increased either by increasing  $l^*$  or decreasing  $d^*$ . In other words, the aspect ratio  $l/d$  of platelets affects the fracture toughness via two mechanisms, namely, the toughening effect of the crack-bridging zone and the enhancement in the effective Young's modulus of nacre.

### 3.3. Effect of interfacial properties

In recognition of the significant role of the interfacial layers (i.e., the organic phase) in the mechanical behavior of nacre, we now examine how the toughening ratio depends on the interfacial properties.

Firstly, the influences of the interfacial strength  $\tau_{\max}$  on the toughening ratio  $\eta$ , the bridging zone length  $\lambda_{\text{br}}^{\text{SS}}$ , and the steady-state toughening ratio  $\eta_{\text{SS}}$  are examined. Fig. 8(a) depicts the variation of  $\eta$  under several representative values of  $\tau_{\max}$  in the range of 10–80 MPa. It is found that a larger value of  $\tau_{\max}$  will yield a higher asymptotic steady-state toughening ratio. As shown in Fig. 8(b), the bridging zone length  $\lambda_{\text{br}}^{\text{SS}}$  decreases with increasing  $\tau_{\max}$ , indicating that stronger interfaces are beneficial for the improvement of fracture toughness. The variation of the steady-state toughening ratio  $\eta_{\text{SS}}$  with respect to the normalized interfacial strength  $\tau_{\max}^*$  is shown in Fig. 8(c). Therefore, the reinforcement of interfacial layers beyond the strength of the original organic matrix is another plausible toughening strategy for nacre.

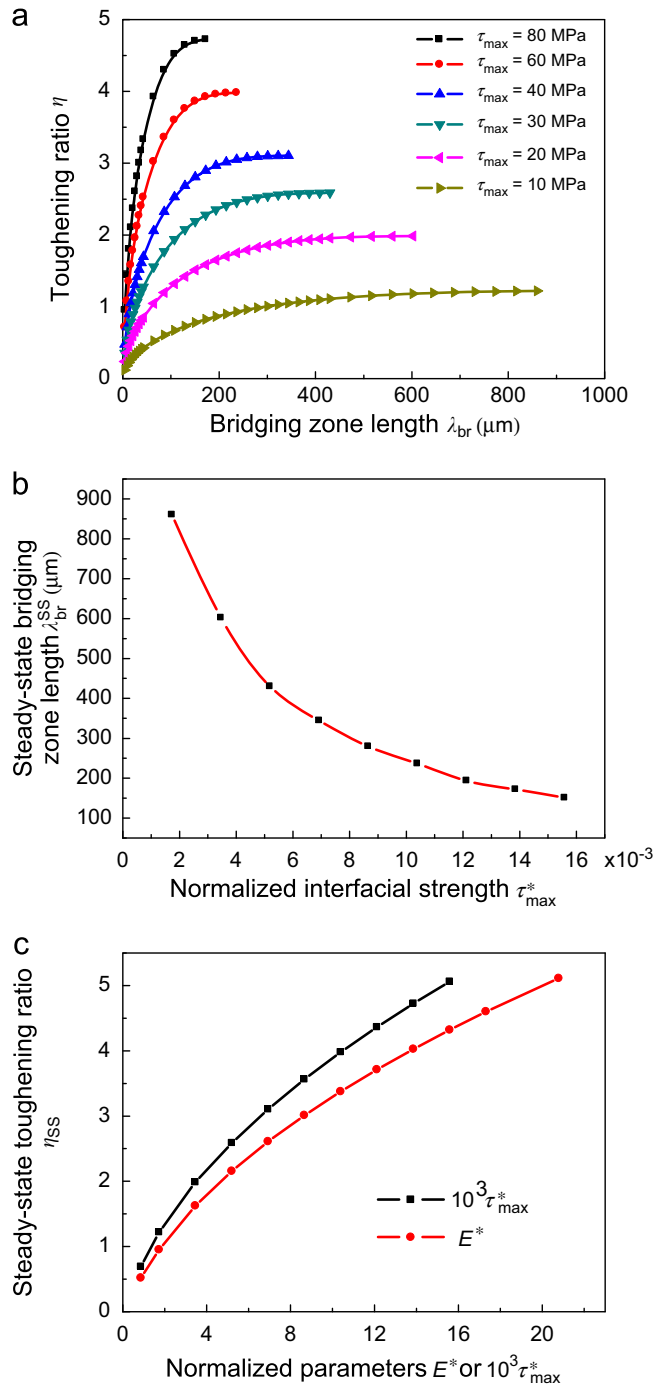


Fig. 8. Effects of the interfacial strength  $\tau_{\max}$  on (a)  $\eta$ -curve, (b)  $\lambda_{\text{br}}^{\text{SS}}$ , and (c)  $\eta_{\text{SS}}$ .

The separation work  $S$ , another key parameter characterizing the energy dissipation of interfacial layers during deformation, also plays an important role in modulating the fracture toughness of nacre. Fig. 9 shows the effect of the normalized separation work  $S^*$  on the toughening ratio  $\eta$ , the bridging zone length  $\lambda_{br}^{SS}$ , and the steady-state toughening ratio  $\eta_{SS}$ . It is seen that a larger separation work  $S^*$  will induce a higher toughening ratio and a longer steady-state bridging zone. The relation between  $\eta_{SS}$  and  $S^*$  is approximately parabolic, as shown in Fig. 9(c). The above results suggest that increasing the dissipative ability of interfacial layers is another efficient way to improve the toughness of nacre.

In fact, several features have been observed in the microstructure of nacre, which can enhance the interfacial strength and energy-dissipative ability, e.g., the surface waviness of platelets (Barthelat and Espinosa, 2007; Barthelat et al., 2007), nanosized asperities (Wang et al., 2001; Bruet et al., 2005; Barthelat et al., 2006), and mineral bridges (Song et al., 2003).

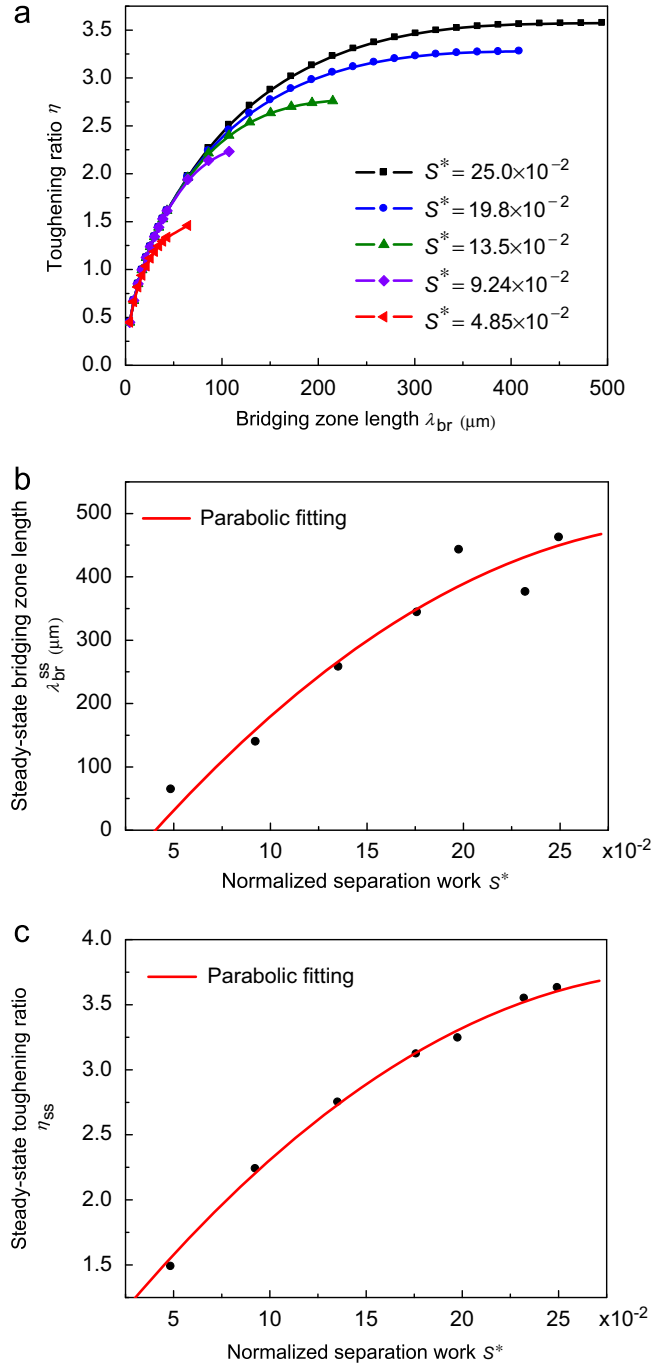


Fig. 9. Effects of the separation work  $S$  of the interfacial cohesive law on (a)  $\eta$ -curve, (b)  $\lambda_{br}^{SS}$ , and (c)  $\eta_{SS}$ .

Our theoretical analyses reveal that these elegant structures at micro and nano scales within the organic layers can greatly help the nacre to possess outstanding macroscopic mechanical properties. This toughening strategy has also been proved to be practicable in artificially synthesized nacre-like materials with high toughness and strength through chemical and physical interfacial grafting technologies (Munch et al., 2008; Launey et al., 2009; Launey et al., 2010).

In addition, it has been recognized that the physiological water content in nacre can help activate the hierarchical failure mechanisms of proteins and other biopolymers in nacre (Smith et al., 1999; Mayer, 2005; Lin and Meyers, 2009) and thus enable the interfacial layers to afford large deformation and significant viscoplastic energy dissipation. Water content affects both the values of  $\tau_{\max}$  and  $S^*$ . Our calculations shows that for a fixed  $\tau_{\max}$ , the fracture toughness increases with rising  $S^*$ . Therefore, the present theoretical model can well elucidate the dependence of the fracture toughness on the water content in nacre (Jackson et al., 1988). This toughening strategy might also be feasible for the design and synthesis of advanced biomimetic materials. Recently, Gao et al. (2011) reported the influence of the interfacial adhesion on the mechanical properties of graphene oxide papers, which have multilayered architecture as nacre. By introducing strengthening and dissipative species between neighboring graphene sheets, they achieved a remarkable improvement on the strength and fracture strain of materials, demonstrating the toughening effect of interfaces as predicted by our theoretical model.

Under specified interface strength  $\tau_{\max}$  and separation work  $S$ , the effects of the two other shape parameters of the interfacial law in Fig. 4,  $\delta_1/\delta_C$  and  $\delta_2/\delta_C$ , on the toughening effect are also considered. When  $\delta_1/\delta_C \neq 0$  and  $\delta_2/\delta_C \neq 0$ , the cohesive law of interfaces has a trapezoidal shape (Fig. 4); when  $\delta_1/\delta_C = 0$  and  $\delta_2/\delta_C = 1$ , it has a square shape; and when  $\delta_1/\delta_C = 0$  and  $\delta_2/\delta_C = 0$ , it has a triangle shape with only a linear softening stage. For several representative thicknesses  $d^*$ , we examined the influences of the shape of the interfacial cohesive law on the toughening ratio  $\eta$ , as shown in Fig. 10(a). Obviously, the shape of the interfacial cohesive law has insignificant influence on the toughening effect and the value of  $\eta_{SS}$  is insensitive to the specific values of  $\delta_1/\delta_C$  and  $\delta_2/\delta_C$  provided that  $\tau_{\max}$  and  $S$  are given. For clarity, the relative differences

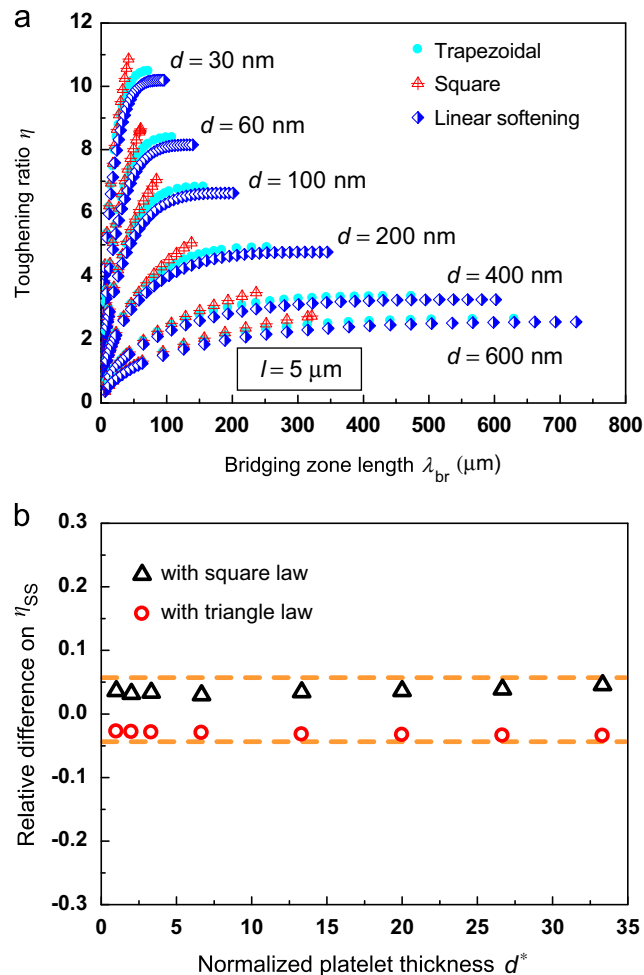


Fig. 10. The influence of the shape of interfacial cohesive laws on (a) the  $\eta$ -curves and (b) the relative differences of  $\eta_{SS}$ .

of the steady-state toughening ratio,  $\eta_{SS}$ , calculated with the two cohesive laws other than the trapezoidal one we used before are given in Fig. 10(b). The absolute values of such relative differences are all below 5%. Therefore,  $\tau_{max}$  and  $S$  are the two primary parameters of interfaces, as claimed for conventional fiber-reinforced composites (Tvergaard and Hutchinson, 1992). The two parameters dominate the bridging toughening effect and the fracture toughness of nacre. This result also validates the generality of our theoretical results based on the trapezoidal interfacial cohesive law in this paper.

### 3.4. Effect of the stacking pattern of platelets

The platelets in nacre have two typical stacking patterns, named columnar nacre and sheet nacre, respectively, depending on the species of the mollusks (Currey, 1977). In the columnar nacre, the terminals of platelets tend to be stacked in columns, as shown in Fig. 11. In sheet nacre, the staggering stacking pattern of platelets is almost random. As in most previous theoretical investigations (Jackson et al., 1988; Ji and Gao, 2004), our attention in the present paper is focused on the ideal stacking pattern of platelets shown in Fig. 2. In fact, our theoretical model can also be used to examine the effect of the stacking pattern of platelets.

For the microstructure of columnar nacre illustrated in Fig. 11, a crack will propagate in a kinked manner, along the shortest propagation path. In this case, the crack-bridging mechanism of platelets is still the dominant toughening mechanism. However, the pullout length of a platelet will equal the overlapping distance  $\Delta$ , rather than  $l$  in Fig. 2. For a mode-I crack in such a nacreous structure, just like that in Fig. 3, the bridging force at the position  $x=\xi_i$  is written as

$$f(\xi_i) = \tau(2\nu(\xi_i))[\Delta - 2\nu(\xi_i)]. \tag{28}$$

In this case, the bridging effect and the crack surface displacement can be calculated by

$$K_I^{br} = -\sqrt{\frac{2}{\pi}} \sum_{i=1}^N \frac{\tau(2\nu(\xi_i))}{\sqrt{\lambda_{br}-\xi_i}} [\Delta - 2\nu(\xi_i)], \tag{29}$$

$$\nu(x) = \frac{4K_I^\infty \sqrt{\lambda_{br}-x}}{\sqrt{2\pi E}} - \frac{2}{\pi E} p.v. \sum_{n=1}^N \ln \frac{\sqrt{\lambda_{br}-x} + \sqrt{\lambda_{br}-\xi_n}}{\sqrt{\lambda_{br}-x} - \sqrt{\lambda_{br}-\xi_n}} \tau(2\nu(\xi_n)) [\Delta - 2\nu(\xi_n)], \tag{30}$$

respectively. Thus, one can predict the fracture toughening of columnar nacre with microstructure shown in Fig. 11. We do not pursue further discussions on this issue here.

### 3.5. Applications to artificial nacreous materials

The results obtained in the preceding subsections show that the crack-bridging toughening effect in nacre is highly sensitive to the platelet sizes. In what follows, we will further correlate the steady-state toughening ratio  $\eta_{SS}$  with the sizes of platelets, which is crucial for the design of artificial nacreous materials. To this end, we simplify Eq. (24) as

$$\eta_{SS} = \left| \frac{K_{ISS}^{br}}{K_I^0} \right| = \Phi(d^*, l^*), \tag{31}$$

where  $\Phi$  is a function to be determined. It should satisfy the following asymptotic conditions: (i) if  $l \rightarrow 0$  or  $d \rightarrow \infty$ , the toughening effect should be negligible, that is,  $\Phi \rightarrow 0$ ; (ii) if  $d \rightarrow 0$  and  $d_{int}$  does not vanish,  $\Phi$  should have a finite value; and

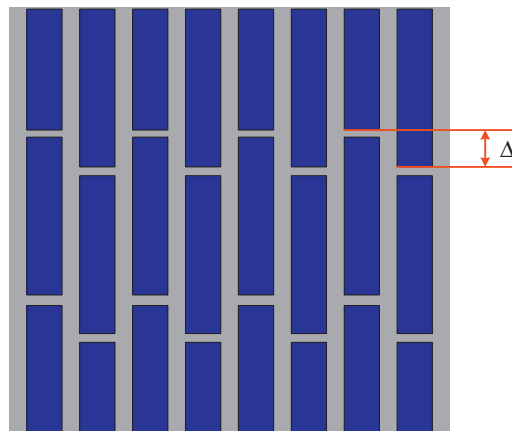


Fig. 11. Schematic of the stacking pattern of platelets in columnar nacre.

(iii)  $\Phi$  should be a monotonically increasing function with respect to  $l$ . These conditions can also be expressed as

$$\lim_{l^* \rightarrow 0} \Phi(d^*, l^*) = 0, \tag{32}$$

$$\lim_{d^* \rightarrow \infty} \Phi(d^*, l^*) = 0, \tag{33}$$

$$\lim_{d^* \rightarrow 0} \Phi(d^*, l^*) = \text{finite value}, \tag{34}$$

$$\Phi(d^*, l^*) \propto l^*. \tag{35}$$

Considering Eqs. (31)–(35), a dimensionless function of  $\eta_{SS}$  is assumed as follows

$$\eta_{SS} = \Phi(d^*, l^*) = \frac{h(l^*)}{g(d^*)} = \frac{\sum_{i=1}^m a_i (l^*)^i}{(d^*)^n + b}, \tag{36}$$

where  $a_i$ ,  $b$ ,  $m$ , and  $n$  are non-dimensional constants. By fitting Eq. (36) to the results in Figs. 5(c) and 6(c), we obtain  $a_1=0.0792$ ,  $a_2=8.58 \times 10^{-4}$ ,  $a_3=-3.07 \times 10^{-6}$ ,  $a_4=3.85 \times 10^{-9}$ ,  $b=1.33$ ,  $m=4$ , and  $n=0.7$ . This relation can well fit all the theoretical results obtained for a broad range of material and geometrical parameters in our model and, thus, could be used to easily predict fracture toughness of materials with nacre-like microstructures.

Fig. 12 gives the contour of  $\eta_{SS}$  calculated from Eq. (36) with respect to the normalized thickness  $d^*$  and length  $l^*$  of platelets in a broad range for natural and artificial nacreous materials. It is illustrated that a certain optimal range of platelet sizes is required to achieve a higher toughening ratio. The greater the expected toughening ratio, the narrower the optimized range of platelet size. Therefore, controlling the platelet sizes in a certain range is necessary to synthesize artificial nacre with high toughness. Such synthesis of artificial nacre may be restricted by available fabrication techniques. However, it is noticed that in different kinds of natural nacre, the platelet sizes vary in a fairly wide range of sizes. This, on one hand, results in dispersion in the fracture toughness among different types of nacre (Rabiei et al., 2010) and, on the other hand, helps to achieve a modest toughening ratio and a robust adaptability to the variations of platelet sizes simultaneously. The relation in Eq. (36) is helpful for understanding the strategy adopted by nature in the selection of building block sizes of nacre and may serve as a guide for the optimal design of nacreous systems by tuning the sizes of platelets.

#### 4. Conclusions

There is mounting experimental evidence that crack-bridging of platelets is one of the most significant toughening mechanisms in nacre, wherein a number of other toughening mechanisms contribute to the high toughness by affecting the process of platelet pullout (Wang et al., 2001; Barthelat and Espinosa, 2007; Espinosa et al., 2009; Rabiei et al., 2010). In this paper, a fracture mechanics model has been proposed to quantitatively evaluate the contribution of the crack-bridging mechanism of platelets to the toughness of nacre. The obtained theoretical results exhibit good comparability with relevant experiments.

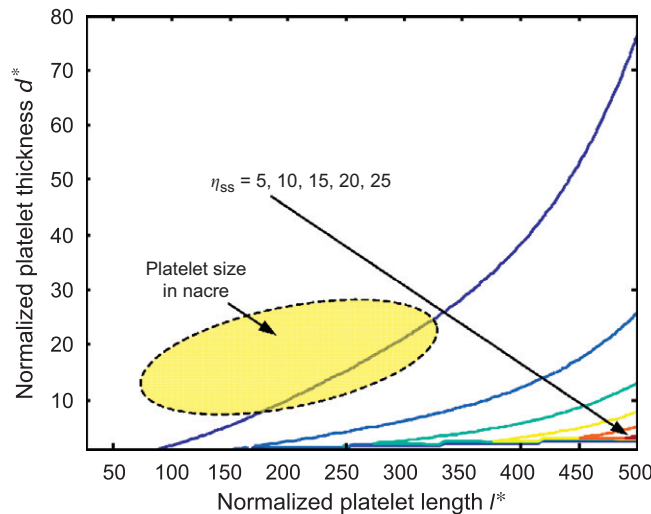


Fig. 12. Contours of the steady-state toughening ratio  $\eta_{SS}$  with respect to normalized platelet sizes. The yellow region illustrates the range of platelet sizes commonly observed in natural nacre.

Our analysis reveals a significant size effect of platelets on the fracture toughness of nacre and provides the optimal ranges for their thickness and length. To achieve higher fracture toughness, the platelets should have a thickness less than one micron, but not thinner than another characteristic value of tens nanometers because overly thin platelets tend to break before being pulled out due to the tensile traction. Thereby, the optimal aspect ratio of platelets can be easily determined. In this range, a larger aspect ratio of platelets is beneficial for the improvement of the toughening effect of cracking bridging.

By comparing different types of cohesive laws, the interfacial strength and energy dissipation of the organic phase are demonstrated to be two dominant parameters for the crack-bridging toughening effect in nacre. Their increase leads to an enhancement of fracture toughness. Our results also confirmed the compatibility between high stiffness and high toughness in natural nacre. Furthermore, the stacking pattern of platelets in the brick-and-mortar microstructure of nacre can also be studied using this theoretical model. Based on the calculation results, we have given a dimensionless function correlating the steady-state toughening ratio with the sizes of platelets. These results not only provide insight into the physical mechanisms underlying the superior mechanical properties of nacre but may also benefit the optimal design of biomimetic materials.

**Acknowledgments**

The supports from the National Natural Science Foundation of China (Grant Nos. 10732050 and 10872116) and 973 Program (2010CB631005 and 2012CB934101) are acknowledged.

**Appendix A. Discrete Cauchy principal value p.v. in Eq. (13)**

In the present model, the bridging forces due to platelets are discretized into a series of concentrated forces,  $f(\xi_i)$ , where  $\xi_i$  is the  $x$  coordinate at the  $i$ th point with  $i=1,2,\dots,N$ . Then the traction  $\sigma_{br}(\xi)$  acting on the crack surface in the bridging zone can be expressed as

$$\sigma_{br}(\xi) = \sum_{i=1}^N \left\{ \tau(\xi) \delta(\xi - \xi_i) \left[ \frac{l}{2} - \nu(\xi) \right] \right\}, \tag{37}$$

where  $\delta(x)$  is the Dirac’s delta function. Substituting Eq. (37) into (12) leads to

$$\begin{aligned} \nu(x) &= \frac{4K_I^\infty \sqrt{\lambda_{br}-x}}{\sqrt{2\pi E}} - \frac{2}{\pi E} P.V. \int_0^{\lambda_{br}} \ln \frac{\sqrt{\lambda_{br}-x} + \sqrt{\lambda_{br}-\xi}}{\left| \sqrt{\lambda_{br}-x} - \sqrt{\lambda_{br}-\xi} \right|} \sigma_{br}(\xi) d\xi \\ &= \frac{4K_I^\infty \sqrt{\lambda_{br}-x}}{\sqrt{2\pi E}} - \frac{2}{\pi E} \sum_{i=1}^N P.V. \int_0^{\lambda_{br}} \ln \frac{\sqrt{\lambda_{br}-x} + \sqrt{\lambda_{br}-\xi}}{\left| \sqrt{\lambda_{br}-x} - \sqrt{\lambda_{br}-\xi} \right|} \tau(\xi) \cdot \left[ \frac{l}{2} - \nu(\xi) \right] \cdot \delta(\xi - \xi_i) d\xi \\ &= \frac{4K_I^\infty \sqrt{\lambda_{br}-x}}{\sqrt{2\pi E}} - \frac{2}{\pi E} \sum_{i=1}^N P.V. \int_{\xi_i-\varepsilon}^{\xi_i+\varepsilon} \ln \frac{\sqrt{\lambda_{br}-x} + \sqrt{\lambda_{br}-\xi}}{\left| \sqrt{\lambda_{br}-x} - \sqrt{\lambda_{br}-\xi} \right|} \tau(\xi) \cdot \left[ \frac{l}{2} - \nu(\xi) \right] \cdot \delta(\xi - \xi_i) d\xi, \end{aligned} \tag{38}$$

where  $\varepsilon > 0$  is a finite positive number. For a given value of  $x$ , the Cauchy principal values in Eq. (38) can be evaluated as follows. Because of the discreteness of bridging forces in our model, we also calculate the Cauchy principal values in a discrete manner.

For  $x \neq \xi_n$  ( $n=1,2,\dots,N$ ), Eq. (38) is simplified as

$$\nu(x) = \frac{4K_I^\infty \sqrt{\lambda_{br}-x}}{\sqrt{2\pi E}} - \frac{2}{\pi E} \sum_{i=1}^N \ln \frac{\sqrt{\lambda_{br}-x} + \sqrt{\lambda_{br}-\xi_i}}{\left| \sqrt{\lambda_{br}-x} - \sqrt{\lambda_{br}-\xi_i} \right|} \tau(\xi_i) \cdot \left[ \frac{l}{2} - \nu(\xi_i) \right]. \tag{39}$$

When  $x = \xi_n$ , we can calculate Eq. (38) invoking to the definition of Cauchy principal value. It becomes

$$\begin{aligned} \nu(\xi_n) &= \frac{4K_I^\infty \sqrt{\lambda_{br}-\xi_n}}{\sqrt{2\pi E}} - \frac{2}{\pi E} \sum_{\substack{i=1 \\ i \neq n}}^N \left\{ \ln \frac{\sqrt{\lambda_{br}-\xi_n} + \sqrt{\lambda_{br}-\xi_i}}{\left| \sqrt{\lambda_{br}-\xi_n} - \sqrt{\lambda_{br}-\xi_i} \right|} \tau(\xi_i) \cdot \left[ \frac{l}{2} - \nu(\xi_i) \right] \right\} \\ &\quad - \frac{2}{\pi E} \left\{ \lim_{a \rightarrow 0^+} \int_{\xi_n-\varepsilon}^{\xi_n-a} \ln \frac{\sqrt{\lambda_{br}-\xi_n} + \sqrt{\lambda_{br}-\xi}}{\left| \sqrt{\lambda_{br}-\xi_n} - \sqrt{\lambda_{br}-\xi} \right|} \tau(\xi) \cdot \left[ \frac{l}{2} - \nu(\xi) \right] \cdot \delta(\xi - \xi_n) d\xi \right\} \\ &\quad - \frac{2}{\pi E} \left\{ \lim_{a \rightarrow 0^+} \int_{\xi_n+a}^{\xi_n+\varepsilon} \ln \frac{\sqrt{\lambda_{br}-\xi_n} + \sqrt{\lambda_{br}-\xi}}{\left| \sqrt{\lambda_{br}-\xi_n} - \sqrt{\lambda_{br}-\xi} \right|} \tau(\xi) \cdot \left[ \frac{l}{2} - \nu(\xi) \right] \cdot \delta(\xi - \xi_n) d\xi \right\} \quad (n = 1, 2, \dots, N). \end{aligned} \tag{40}$$

Eq. (40) is the full expression of Eq. (15); however, the two limits in Eq. (40) are difficult to be evaluated analytically. Therefore, an approximation is made in order to get an explicit form of Eq. (40). By shifting the peak position of Dirac’s

delta function from  $\xi_n$  to  $\xi_n + \zeta$ , where  $\zeta = 10^{-9} < 0.01\xi_n$  is a small positive constant, the two limits in Eq. (40) are approximately expressed as

$$\lim_{a \rightarrow 0^+} \int_{\xi_n - \varepsilon}^{\xi_n - a} \ln \frac{\sqrt{\lambda_{br} - \xi_n} + \sqrt{\lambda_{br} - \xi}}{\sqrt{\lambda_{br} - \xi_n} - \sqrt{\lambda_{br} - \xi}} \tau(\xi) \cdot \left[ \frac{1}{2} - \nu(\xi) \right] \cdot \delta(\xi - \xi_n - \zeta) d\xi \approx 0, \quad (41)$$

$$\begin{aligned} & \lim_{a \rightarrow 0^+} \int_{\xi_n + a}^{\xi_n + \varepsilon} \ln \frac{\sqrt{\lambda_{br} - \xi_n} + \sqrt{\lambda_{br} - \xi}}{\sqrt{\lambda_{br} - \xi_n} - \sqrt{\lambda_{br} - \xi}} \tau(\xi) \cdot \left[ \frac{1}{2} - \nu(\xi) \right] \cdot \delta(\xi - \xi_n - \zeta) d\xi \\ &= \ln \frac{\sqrt{\lambda_{br} - \xi_n} + \sqrt{\lambda_{br} - (\xi_n + \zeta)}}{\sqrt{\lambda_{br} - \xi_n} - \sqrt{\lambda_{br} - (\xi_n + \zeta)}} \tau(\xi_n + \zeta) \cdot \left[ \frac{1}{2} - \nu(\xi_n + \zeta) \right] \approx \ln \frac{\sqrt{\lambda_{br} - \xi_n} + \sqrt{\lambda_{br} - (\xi_n + \zeta)}}{\sqrt{\lambda_{br} - \xi_n} - \sqrt{\lambda_{br} - (\xi_n + \zeta)}} \tau(\xi_n) \cdot \left[ \frac{1}{2} - \nu(\xi_n) \right], \end{aligned} \quad (42)$$

respectively. Thus, Eq. (40) reduces to

$$\begin{aligned} \nu(\xi_n) &= \frac{4K_I^\infty \sqrt{\lambda_{br} - \xi_n}}{\sqrt{2\pi E}} - \frac{2}{\pi E} \sum_{\substack{i=1 \\ i \neq n}}^N \left\{ \ln \frac{\sqrt{\lambda_{br} - \xi_n} + \sqrt{\lambda_{br} - \xi_i}}{\sqrt{\lambda_{br} - \xi_n} - \sqrt{\lambda_{br} - \xi_i}} \tau(\xi_i) \cdot \left[ \frac{1}{2} - \nu(\xi_i) \right] \right\} \\ &\quad - \frac{2}{\pi E} \ln \frac{\sqrt{\lambda_{br} - \xi_n} + \sqrt{\lambda_{br} - (\xi_n + \zeta)}}{\sqrt{\lambda_{br} - \xi_n} - \sqrt{\lambda_{br} - (\xi_n + \zeta)}} \tau(\xi_n) \cdot \left[ \frac{1}{2} - \nu(\xi_n) \right]. \end{aligned} \quad (43)$$

The term  $p.v.$  in Eq. (13) stands for the approximate summation method described above. In our study, we substitute Eq. (43) into (15) in order to calculate the crack opening displacements with the effect of crack bridging.

## References

- Barthelat, F., 2007. Biomimetics for next generation materials. *Philos. Trans. R. Soc. A* 365, 2907–2919.
- Barthelat, F., 2010. Nacre from mollusk shells: a model for high-performance structural materials. *Bioinsp. Biomim.* 5, 035001.
- Barthelat, F., Espinosa, H.D., 2007. An experimental investigation of deformation and fracture of nacre — mother of pearl. *Exp. Mech.* 47, 311–324.
- Barthelat, F., Li, C.M., Comi, C., Espinosa, H.D., 2006. Mechanical properties of nacre constituents and their impact on mechanical performance. *J. Mater. Res.* 21, 1977–1986.
- Barthelat, F., Rabiei, R., 2011. Toughness amplification in natural composites. *J. Mech. Phys. Solids* 59, 829–840.
- Barthelat, F., Zhu, D., 2011. A novel biomimetic materials duplicating the structure and mechanics of natural nacre. *J. Mater. Res.* 26, 1203–1215.
- Barthelat, F., Tang, H., Zavattieri, P.D., Li, C.M., Espinosa, H.D., 2007. On the mechanics of mother-of-pearl: a key feature in the material hierarchical structure. *J. Mech. Phys. Solids* 55, 306–337.
- Bekah, S., Rabiei, R., Barthelat, F., 2011. Structure, scaling and performance of natural micro- and nanocomposites. *BioNanoSci* 1, 53–61.
- Bhushan, B., 2009. Biomimetics: lessons from nature — an overview. *Philos. Trans. R. Soc. A* 367, 1445–1486.
- Bonderer, L.J., Studart, A.R., Gauckler, L.J., 2008. Bioinspired design and assembly of platelet reinforced polymer films. *Science* 319, 1069–1073.
- Broberg, K.B., 1999. *Cracks and Fracture*. Academic Press, UK.
- Bruet, B.J.F., Qi, H.J., Boyce, M.C., Panas, R., Tai, K., Frick, L., Ortiz, C., 2005. Nanoscale morphology and indentation of individual nacre tablets from the gastropod mollusc *Trochus niloticus*. *J. Mater. Res.* 20, 2400–2419.
- Budiansky, B., Amazigo, J.C., 1989. Toughening by aligned, frictionally constrained fibers. *J. Mech. Phys. Solids* 37, 93–109.
- Burghard, Z., Tucid, A., Jeurgens, L.P.H., Hoffmann, R.C., Bill, J., Aldinger, F., 2006. Nanomechanical properties of bioinspired organic–inorganic composite films. *Adv. Mater.* 19, 970–974.
- Chan, H.M., 1997. Layered ceramics: processing and mechanical behavior. *Annu. Rev. Mater. Sci.* 27, 249–282.
- Cho, S.S., Park, S., 2004. Finite element modeling of adhesive contact using molecular potential. *Tribol. Int.* 37, 763–769.
- Currey, J.D., 1977. Mechanical properties of mother of pearl in tension. *Proc. R. Soc. Lond. B* 196, 443–463.
- Espinosa, H.D., Juster, A.L., Latourte, F.J., Loh, O.Y., Gregoire, D., Zavattieri, P.D., 2011. Tablet-level origin of toughening in abalone shells and translation to synthetic composite materials. *Nat. Commun.* 2, 173.
- Espinosa, H.D., Rim, J.E., Barthelat, F., Buehler, M.J., 2009. Merger of structure and material in nacre and bone — perspectives on de novo biomimetic materials. *Prog. Mater. Sci.* 54, 1059–1100.
- Evans, A.G., 1990. Perspective on the development of high-toughness ceramics. *J. Am. Ceram. Soc.* 73, 187–206.
- Evans, A.G., Suo, Z., Wang, R.Z., Aksay, I.A., He, M.Y., Hutchinson, J.W., 2001. Model for the robust mechanical behavior of nacre. *J. Mater. Res.* 16, 2475–2484.
- Fleischli, F.D., Dietiker, M., Borgia, C., Spolenak, R., 2008. The influence of internal length scales on mechanical properties in natural nanocomposites: a comparative study on inner layers of seashells. *Acta Biomater.* 4, 1694–1706.
- Fratzl, P., Gupta, H.S., Fischer, F.D., Kolednik, O., 2007. Hindered crack propagation in materials with periodically varying Young's modulus — lessons from biological materials. *Adv. Mater.* 19, 2657–2661.
- Fratzl, P., Weinkamer, R., 2007. Nature's hierarchical materials. *Prog. Mater. Sci.* 52, 1263–1334.
- Gao, H., Ji, B., 2003. Modeling fracture in nanomaterials via a virtual internal bond method. *Eng. Fract. Mech.* 70, 1777–1791.
- Gao, H., Ji, B., Jager, I.L., Arzt, E., Fratzl, P., 2003. Materials become insensitive to flaws at nanoscale: lessons from nature. *Proc. Natl. Acad. Sci. USA* 100, 5597–5600.
- Gao, H., 2006. Application of fracture mechanics concepts to hierarchical biomechanics of bone and bone-like materials. *Int. J. Fract.* 138, 101–137.
- Gao, Y., Liu, L.Q., Zu, S.Z., Peng, K., Zhou, D., Han, B.H., Zhang, Z., 2011. The effect of interlayer adhesion on the mechanical behaviors of macroscopic graphene oxide paper. *ACS Nano* 5, 2134–2141.
- Hutchinson, J.W., 1987. Crack tip shielding by microcracking in brittle solids. *Acta Metall.* 35, 1605–1619.
- Jackson, A.P., Vincent, J.F.V., Turner, R.M., 1988. The mechanical design of nacre. *Proc. R. Soc. Lond. B* 234, 415–440.
- Ji, B., Gao, H., 2004. Mechanical properties of nanostructure of biological materials. *J. Mech. Phys. Solids* 52, 1963–1990.
- Ji, B., Gao, H., 2010. Mechanical principles of biological nanocomposites. *Annu. Rev. Mater. Res.* 40, 77–100.
- Kamat, S., Su, X., Ballarini, R., Heuer, A.H., 2000. Structural basis for the fracture toughness of the shell of the conch *Strombus gigas*. *Nature* 405, 1036–1040.
- Launey, M.E., Munch, E., Alem, D.H., Barth, H.B., Saiz, E., Tomsia, A.P., Ritchie, R.O., 2009. Designing highly toughened hybrid composites through nature-inspired hierarchical complexity. *Acta Mater.* 57, 2919–2932.
- Launey, M.E., Ritchie, R.O., 2009. On the fracture toughness of advanced materials. *Adv. Mater.* 21, 1–8.

- Launey, M.E., Munch, E., Alsem, D.H., Saiz, E., Tomsia, A.P., Ritchie, R.O., 2010. A novel biomimetic approach to the design of high-performance ceramic-metal composites. *J. R. Soc. Interface* 7, 741–753.
- Li, B.W., Zhao, H.P., Feng, X.Q., Guo, W.W., Shan, S.C., 2010. Experimental study on the mechanical properties of the horn sheaths from cattle. *J. Exp. Biol.* 213, 479–486.
- Li, H., Jiang, W.G., Feng, X.Q., 2012. Normal impact of adhesive microparticles with a thin-film/substrate system: a numerical study. *Comput. Mater. Sci.* 60, 130–136.
- Li, X.D., Chang, W.C., Chao, Y.J., Wang, R.Z., Chang, M., 2004. Nanoscale structural and mechanical characterization of a natural nanocomposite material: the shell of red abalone. *Nano Lett.* 4, 613–617.
- Lin, A., Meyers, M.A., 2005. Growth and structure in abalone shell. *Mater. Sci. Eng. A* 390, 27–41.
- Lin, A., Meyers, M.A., 2009. Interfacial shear strength in abalone nacre. *J. Mech. Behav. Biomed. Mater.* 2, 607–612.
- Lu, Z.X., Yu, S.W., Wang, X.Y., Feng, X.Q., 2007. Effect of interfacial slippage in peel test: Theoretical model. *Eur. Phys. J. E* 23, 67–76.
- Luz, G.M., Mano, J.F., 2009. Biomimetic design of materials and biomaterials inspired by the structure of nacre. *Philos. Trans. R. Soc. A* 367, 1587–1605.
- Mai, Y.W., Lawn, B.R., 1987. Crack-interface grain bridging as a fracture resistance mechanism in ceramics: II, theoretical fracture mechanics model. *J. Am. Ceram. Soc.* 70, 289–294.
- Mayer, G., 2005. Rigid biological systems as models for synthetic composites. *Science* 310, 1144–1147.
- Mayer, G., Sarikaya, M., 2002. Rigid biological composite materials: structural examples for biomimetic design. *Exp. Mech.* 42, 395–403.
- McMeeking, R.M., Evans, A.G., 1982. Mechanics of transformation-toughening in brittle materials. *J. Am. Ceram. Soc.* 65, 242–246.
- Menig, R., Meyers, M.H., Meyers, M.A., Vecchio, K.S., 2000. Quasi-static and dynamic mechanical response of *Haliotis rufescens* (Abalone) shells. *Acta Mater.* 48, 2383–2398.
- Meyers, M.A., Chen, P.Y., Lin, A., Seki, Y., 2008. Biological materials: structure and mechanical properties. *Prog. Mater. Sci.* 53, 1–206.
- Munch, E., Launey, M.E., Alsem, D.H., Saiz, E., Tomsia, A.P., Ritchie, R.O., 2008. Tough, bio-inspired hybrid materials. *Science* 322, 1516–1520.
- Nassif, N., Pinna, N., Gerhke, N., Antonietti, M., Jäger, C., Cölfen, H., 2005. Amorphous layer around aragonite platelets in nacre. *Proc. Natl. Acad. Sci. USA* 102, 12653–12655.
- Nukala, K.P.V.V., Šimunović, S., 2005. Statistical physics models for nacre fracture simulation. *Phys. Rev. E* 72, 041919.
- Okumura, K., de Gennes, P.G., 2001. Why is nacre strong? Elastic theory and fracture mechanics for biocomposites with stratified structures. *Eur. Phys. J. E* 4, 121–127.
- Okumura, K., 2002. Why is nacre strong? II. Remaining mechanical weakness for cracks propagating along the sheets. *Eur. Phys. J. E* 7, 303–310.
- Okumura, K., 2003. Enhanced energy of parallel fractures in nacre-like composite materials. *Europhys. Lett.* 63, 701–707.
- Podsiadlo, P., Kaushik, A.K., Arruda, E.M., Waas, A.M., Shim, B.S., Xu, J., Nandivada, H., Pumphlin, B.G., Lahann, J., Ramamoorthy, A., Kotov, N.A., 2007. Ultrastrong and stiff layered polymer nanocomposites. *Science* 318, 80–83.
- Rabiei, R., Bekah, S., Barthelat, F., 2010. Failure mode transition in nacre and bone-like materials. *Acta Biomater.* 6, 4081–4089.
- Ritchie, R.O., 2011. The conflicts between strength and toughness. *Nat. Mater.* 10, 817–822.
- Sarikaya, M., 1994. An introduction to biomimetics: a structural viewpoint. *Microsc. Res. Tech.* 27, 360–375.
- Schäffer, T.E., Ionescu-Zanetti, C., Proksch, R., Fritz, M., Walters, D.A., Almqvist, N., Zaremba, C.M., Belcher, A.M., Smith, B.L., Stucky, G.D., Morse, D.E., Hansma, P.K., 1997. Does abalone nacre form by heteroepitaxial nucleation or by growth through mineral bridges? *Chem. Mater.* 9, 1731–1740.
- Smith, B.L., Schäffer, T.E., Viani, M., Tompson, J.B., Frederick, N.A., Kindt, J., Belcher, A., Stucky, G.D., Morese, D.E., Hansma, P.K., 1999. Molecular mechanistic origin of the toughness of natural adhesives, fibres and composites. *Nature* 399, 761–763.
- Song, F., Bai, Y.L., 2003. Effects of nanostructures on the fracture strength of the interfaces in nacre. *J. Mater. Res.* 18, 1741–1744.
- Song, F., Soh, A.K., Bai, Y.L., 2003. Structural and mechanical properties of the organic matrix layers of nacre. *Biomaterials* 24, 3623–3631.
- Song, F., Zhou, J.B., Xu, X.H., Xu, Y., Bai, Y.L., 2008. Effect of a negative Poisson ratio in the tension of ceramics. *Phys. Rev. Lett.* 100, 245502.
- Tada, H., Paris, P.C., Irwin, G.R., 1985. *The Stress Analysis of Cracks Handbook*. Paris Productions.
- Tang, H., Barthelat, F., Espinosa, H.D., 2007. An elasto-viscoplastic interface model for investigating the constitutive behavior of nacre. *J. Mech. Phys. Solids* 55, 1410–1438.
- Tang, Z.Y., Kotov, N.A., Magonov, S., Ozturk, B., 2003. Nanostructured artificial nacre. *Nat. Mater.* 2, 413–418.
- Tvergaard, V., Hutchinson, J.W., 1992. The relation between crack growth resistance and fracture process parameters in elastic-plastic solids. *J. Mech. Phys. Solids* 40, 1377–1397.
- Tvergaard, V., Hutchinson, J.W., 1993. The influence of plasticity on mixed mode interface toughness. *J. Mech. Phys. Solids* 41, 1119–1135.
- Wang, R.Z., Suo, Z., Evans, A.G., Yao, A., Aksay, I.A., 2001. Deformation mechanisms in nacre. *J. Mater. Res.* 16, 2485–2493.
- Wei, Y.G., Hutchinson, J.W., 1998. Interface strength, work of adhesion and plasticity in the peel test. *Int. J. Fract.* 93, 315–333.
- Zhang, Z.Q., Liu, B., Huang, Y., Huang, K.C., Gao, H., 2010. Mechanics of unidirectional nanocomposites with non-uniformly or randomly staggered platelet distribution. *J. Mech. Phys. Solids* 58, 1646–1660.
- Zhang, Z.Q., Zhang, Y.W., Gao, H., 2011. On optimal hierarchy of load-bearing biological materials. *Proc. R. Soc. B* 278, 519–525.
- Zhao, H.P., Feng, X.Q., Yu, S.W., Cui, W.Z., Zou, F.Z., 2005. Mechanical properties of silkworm cocoons. *Polymer* 46, 9192–9201.
- Zhao, H.P., Feng, X.Q., Gao, H.J., 2007. Ultrasonic technique for extracting nanofibers from nature materials. *Appl. Phys. Lett.* 90, 073112.